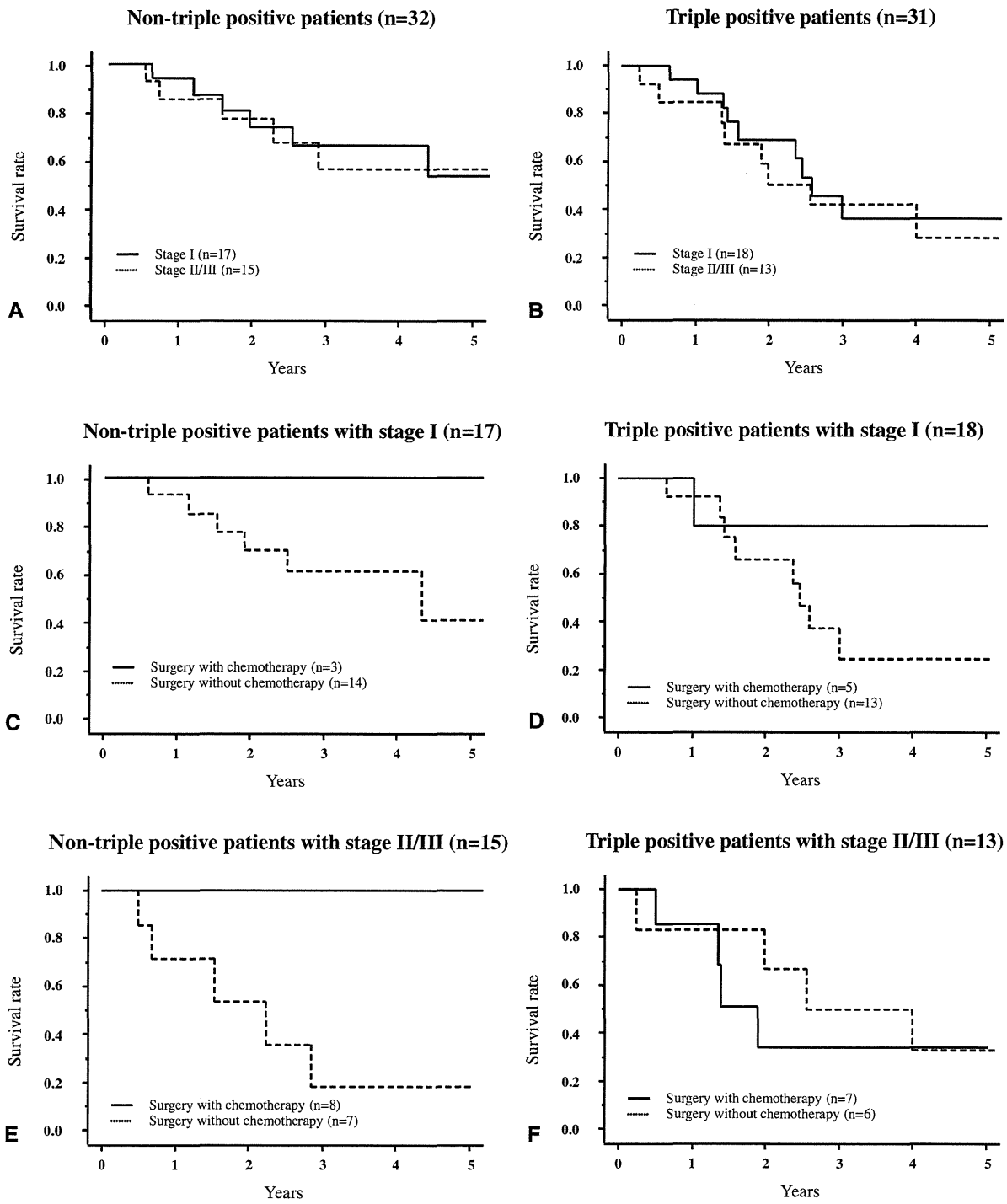

FIGURE 2. A, Comparison of stage-specific survival of patients with non–triple-positive large cell neuroendocrine carcinoma. B, Comparison of stage-specific survival of patients with triple-positive large cell neuroendocrine carcinoma. C, Comparison of survival of patients with stage I nontriple-positive disease who underwent surgery with perioperative chemotherapy and those who underwent surgery without perioperative chemotherapy. D, Comparison of survival of patients with stage I triple-positive who underwent surgery with perioperative chemotherapy and those who underwent surgery without perioperative chemotherapy. E, Comparison of survival of patients with stage II/III non–triple-positive disease who underwent surgery with perioperative chemotherapy and those who underwent surgery without perioperative chemotherapy. F, Comparison of survival of patients with stage II/III triple-positive disease who underwent surgery with perioperative chemotherapy and those who underwent surgery without perioperative chemotherapy. *Non–triple positive,* Negative for 1 or 2 neuroendocrine markers (synaptophysin, chromogranin A, and neural cell adhesion molecule); *Triple positive,* positive for synaptophysin, chromogranin A, and neural cell adhesion molecule.

that LCNEC does not have all 3 proteins. It was reported that neuroendocrine markers are often negative in poorly differentiated neuroendocrine cancers,[18] and it is estimated that LCNEC in the non–triple-positive group tended to be poorly differentiated and associated with a poor prognosis. Our results have demonstrated that the 5-year survival rate of patients who did not undergo perioperative chemotherapy in the non–triple-positive group was 34.5%. The addition of perioperative chemotherapy improved the prognosis of LCNEC in the non–triple-positive group but did not improve the prognosis of LCNEC in the triple-positive group. We considered that LCNEC might become resistant to chemotherapy through coexistence and mutual interaction of synaptophysin, chromogranin A, and NCAM and might lose the ability to resist because of the deficiency of the mutual interaction, owing to a lack of any of the 3 proteins.

Various studies have analyzed LCNEC's prognostic factors using other immunohistochemical staining and gene expression profiles.[19-21] However, no report has more clearly demonstrated the sensitivity of pulmonary LCNEC to perioperative chemotherapy than has our study. Moreover, it is also considered valuable that we can describe this result with 3 well-known biomarkers that are necessary for the diagnosis of pulmonary LCNEC. Furthermore, it was reported that carcinoids that exhibit good prognosis have a low response rate to chemotherapy and SCLCs that show a poor prognosis have a high initial response rate to chemotherapy.[18,22] Considered with our results, it is likely that triple-positive LCNEC was rich in neuroendocrine character, similar to carcinoids, and the non–triple-positive LCNECs were poor in neuroendocrine character, similar to SCLCs.

In the present study, antibody staining was designated as negative when none of the tumor cells were stained and as positive when any degree of immunoreactivity was found. We determined the cutoff value using the following scoring system: 0, no positive cells; 1+, less than 10% of cells positive; 2+, 10% to 50% of cells positive; and 3+, more than 50% of cells positive. From this analysis, the optimal cutoff, defined as the value that best separated a poor prognostic group from a better prognostic group, was nonimmunoreactive (negative) vs immunoreactive (positive) for the neuroendocrine markers. The evaluation separating "positive" from "negative," without any counting of cells, was easily and quickly performed with high reproducibility, which could be an advantage in possible future use in the clinical setting.

At present, most LCNECs are diagnosed using surgically resected specimens and rarely using biopsy or cytology specimens. Almost all publications concerning resected LCNEC have been based on the retrospective analyses of surgical specimens.[23] We used postoperative specimens to diagnose pulmonary LCNEC and to categorize them as either triple positive or non–triple positive. However, it would be difficult to categorize LCNEC according to our criteria using small biopsy specimens or cytologic specimens because heterogeneity and focal and scattered positivity of immunostaining against the neuroendocrine markers are not unusual. Therefore, this method might not be applicable for neoadjuvant chemotherapy.

Regarding the perioperative chemotherapy regimens for pulmonary LCNEC, platinum-based regimens that include etoposide (VP-16) or irinotecan (CPT-11), which are standard for SCLC, are more effective than other platinum-based regimens for NSCLCs, because pulmonary LCNEC is genetically and immunohistochemically more similar to SCLC than to NSCLC.[10,24,25] In our study, 10 (43%) of the 23 patients underwent a platinum-based regimen that included VP-16 or CPT-11. In addition, 3 (27%) of 11 patients in the non–triple-positive group received a platinum-based regimen that included VP-16 or CPT-11, in contrast to 7 (58%) of 12 patients in the triple-positive group. We considered that our result (ie, the sensitivity of LCNEC to perioperative chemotherapy in the non–triple-positive group), was not affected by the regimen of chemotherapy that included VP-16 or CPT-11.

Evidence is increasing that surgical resection alone is insufficient as treatment of LCNEC, even for stage I disease, and perioperative platinum-based chemotherapy might provide a survival advantage for patients with stage I LCNEC.[9,10] Our results have demonstrated that patients with stage I LCNEC tended to benefit from perioperative chemotherapy, although we failed to demonstrate a significant difference because only a small number of patients with stage I received perioperative chemotherapy. In the patients with stage I, perioperative chemotherapy tended to be associated with longer survival in the non–triple-positive group, as well as in the triple-positive group.

Although we acknowledge our study's limitations (a small number of subjects and short-term follow-up), our results have demonstrated that perioperative chemotherapy can enhance survival for the patients in the non–triple-positive group, although no correlation was seen between chemotherapy and survival in the triple-positive group. We believe these preliminary results are a reasonable rationale for a larger study to determine the correlation between chemotherapy response and neuroendocrine immunoreactivity in patients with LCNEC.

CONCLUSIONS

Our results have suggested that perioperative chemotherapy can be an important therapeutic option in the treatment of pulmonary LCNEC, particularly in the non–triple-positive patients. In the future, prospective multi-institutional studies with larger sample sizes should be conducted to verify the validity of our findings. Continued studies, including molecular studies, are also important to further improve the treatment stratification of patients with LCNEC.

References

1. Travis WD, Linnoila RI, Tsokos MG, Hitchcock CL, Cutler GB Jr, Nieman L, et al. Neuroendocrine tumors of the lung with proposed criteria for large-cell neuroendocrine carcinoma: an ultrastructural, immunohistochemical, and flow cytometric study of 35 cases. *Am J Surg Pathol.* 1991;15:529-53.
2. Travis WD, Corrin B, Shimosato Y. Histological typing of lung and pleural tumors. In: World Health Organization International Histological Classification of Tumors. 3rd ed. Berlin: Springer-Verlag; 1999.
3. Cooper WA, Thourani VH, Gal AA, Lee RB, Mansour KA, Miller JI. The surgical spectrum of pulmonary neuroendocrine neoplasms. *Chest.* 2001;119:14-8.
4. Iyoda A, Hiroshima K, Toyozaki T, Haga Y, Fujisawa T, Ohwada H. Clinical characterization of pulmonary large cell neuroendocrine carcinoma and large cell carcinoma with neuroendocrine morphology. *Cancer.* 2001;91: 1992-2000.
5. Takei H, Asamura H, Maeshima A, Suzuki K, Kondo H, Niki T, et al. Large cell neuroendocrine carcinoma of the lung: a clinicopathologic study of eighty-seven cases. *J Thorac Cardiovasc Surg.* 2002;124:285-92.
6. Battafarano RJ, Fernandez FG, Ritter J, Meyers BF, Guthrie TJ, Cooper JD, et al. Large cell neuroendocrine carcinoma: an aggressive form of non-small cell lung cancer. *J Thorac Cardiovasc Surg.* 2005;130:166-72.
7. Asamura H, Kameya T, Matsuno Y, Noguchi M, Tada H, Ishikawa Y, et al. Neuroendocrine neoplasms of the lung: a prognostic spectrum. *J Clin Oncol.* 2006; 24:70-6.
8. Iyoda A, Hiroshima K, Toyozaki T, Haga Y, Baba M, Fujisawa T, et al. Adjuvant chemotherapy for large cell carcinoma with neuroendocrine features. *Cancer.* 2001;92:1108-12.
9. Iyoda A, Hiroshima K, Moriya Y, Takiguchi Y, Sekine Y, Shibuya K, et al. Prospective study of adjuvant chemotherapy for pulmonary large cell neuroendocrine carcinoma. *Ann Thorac Surg.* 2006;82:1802-7.
10. Saji H, Tsuboi M, Matsubayashi J, Miyajima K, Shimada Y, Imai K, et al. Clinical response of large cell neuroendocrine carcinoma of the lung to perioperative adjuvant chemotherapy. *Anticancer Drugs.* 2010;21:89-93.
11. Sarkaria IS, Iyoda A, Roh MS, Sica G, Kuk D, Sima CS, et al. Neoadjuvant and adjuvant chemotherapy in resected pulmonary large cell neuroendocrine carcinomas: a single institution experience. *Ann Thorac Surg.* 2011;92:1180-6.
12. Sobin L, Wittekind CH, eds. *TNM classification of malignant tumours.* 6th ed. New York: Wiley-Liss; 2002. p. 99-103.
13. Guinee DG Jr, Fishback NF, Koss MN, Abbondanzo SL, Travis WD. The spectrum of immunohistochemical staining of small-cell lung carcinoma in specimens from transbronchial and open-lung biopsies. *Am J Clin Pathol.* 1994;102:406-14.
14. González-Aragoneses F, Moreno-Mata N, Cebollero-Presmanes M, García-Yuste M, Cañizares-Carretero MA, Molins-López-Rodó L, et al. Prognostic significance of synaptophysin in stage I of squamous carcinoma and adenocarcinoma of the lung. *Cancer.* 2007;110:1776-81.
15. Leung ASY, Cooper K, Leung FJWM. Manual of Diagnostic Antibodies for Immunohistology. London; Greenwich Medical Media: 1999:307.
16. Gosney JR, Gosney MA, Lye M, Butt SA. Reliability of commercially available immsunocytochemical markers for identification of neuroendocrine differentiation in bronchoscopic biopsies of bronchial carcinoma. *Thorax.* 1995;50:116-20.
17. Ionescu DN, Treaba D, Gilks CB, Leung S, Renouf D, Laskin J, et al. Nonsmall cell lung carcinoma with neuroendocrine differentiation—an entity of no clinical or prognostic significance. *Am J Surg Pathol.* 2007;31:26-32.
18. Gustafsson BI, Kidd M, Chan A, Malfertheiner MV, Modlin IM. Bronchopulmonary neuroendocrine tumors. *Cancer.* 2008;113:5-21.
19. Faggiano A, Sabourin JC, Ducreux M, Lumbroso J, Duvillard P, Leboulleux S, et al. Pulmonary and extrapulmonary poorly differentiated large cell neuroendocrine carcinomas: diagnostic and prognostic features. *Cancer.* 2007;110:265-74.
20. Harada M, Yokose T, Yoshida J, Nishiwaki Y, Nagai K. Immunohistochemical neuroendocrine differentiation is an independent prognostic factor in surgically resected large cell carcinoma of the lung. *Lung Cancer.* 2002;38:177-84.
21. Beasley MB, Lantuejoul S, Abbondanzo S, Chu WS, Hasleton PS, Travis WD, et al. The P16/cyclin D1/Rb pathway in neuroendocrine tumors of the lung. *Hum Pathol.* 2003;34:136-42.
22. Turrisi AT III, Kim K, Blum R, Sause WT, Livingston RB, Komaki R, et al. Twice-daily compared with once-daily thoracic radiotherapy in limited small-cell lung cancer treated concurrently with cisplatin and etoposide. *N Engl J Med.* 1999;340:265-71.
23. Travis WD, Rush W, Flieder DB, Falk R, Fleming MV, Gal AA, et al. Survival analysis of 200 pulmonary neuroendocrine tumors with clarification of criteria for atypical carcinoid and its separation from typical carcinoid. *Am J Surg Pathol.* 1998;22:934-44.
24. Rossi G, Cavazza A, Marchioni A, Longo L, Migaldi M, Sartori G, et al. Role of chemotherapy and the receptor tyrosine kinases KIT, PDGFRalpha, PDGFRbeta, and Met in large-cell neuroendocrine carcinoma of the lung. *J Clin Oncol.* 2005; 23:8774-85.
25. Rusch VW, Klimstra DS, Venkatraman ES. Molecular markers help characterize neuroendocrine lung tumors. *Ann Thorac Surg.* 1996;62:798-809. 710.

Lung Cancer 79 (2013) 77–82

Contents lists available at SciVerse ScienceDirect

Lung Cancer

journal homepage: www.elsevier.com/locate/lungcan

Psf3 is a prognostic biomarker in lung adenocarcinoma

Daisuke Hokka[a], Yoshimasa Maniwa[a,*], Shinya Tane[a], Wataru Nishio[a], Masahiro Yoshimura[a], Yutaka Okita[b], Chiho Ohbayashi[c], Yasuhiro Sakai[c], Xue Chen[d], Yoshitake Hayashi[d]

[a] Division of Thoracic Surgery, Department of Surgery, Kobe University Graduate School of Medicine, 7-5-2, Kusunoki-cho, Chuo-ku, Kobe-city, 650-0017, Japan
[b] Division of Cardiovascular Surgery, Department of Surgery, Kobe University Graduate School of Medicine, 7-5-2, Kusunoki-cho, Chuo-ku, Kobe-city, 650-0017, Japan
[c] Division of Cancer Pathology, Department of Pathology, Kobe University Graduate School of Medicine, 7-5-2, Kusunoki-cho, Chuo-ku, Kobe-city, 650-0017, Japan
[d] Division of Molecular Medicine and Medical Genetics, Department of Pathology, Kobe University Graduate School of Medicine, 7-5-2, Kusunoki-cho, Chuo-ku, Kobe-city, 650-0017, Japan

ARTICLE INFO

Article history:
Received 13 July 2012
Received in revised form
26 September 2012
Accepted 3 October 2012

Keywords:
Psf3
GINS complex
Lung adenocarcinoma
Prognostic biomarker
Ki67
Adjuvant therapy

ABSTRACT

Psf3 is a member of the evolutionarily conserved heterotetrameric complex GINS (Go-Ichi-Ni-San), which consists of Sld5, Psf1, Psf2, and Psf3. Previous studies have suggested that some GINS complex members are upregulated in cancer, but the status of Psf3 expression in lung adenocarcinoma has not been investigated. The objective of the current study was to determine whether Psf3 plays a role in lung adenocarcinoma by investigating clinical samples. We investigated the status of Psf3 expression in cancer cells of 125 consecutive resected lung adenocarcinomas by immunohistochemistry. Increased Psf3 expression was observed in 27 (21.6%) of the 125 cases. Further, univariate analysis and log-rank test indicated a significant association between Psf3 expression and lower overall survival rate ($P=0.0001$ and $P<0.0001$, respectively). Multivariate analysis also indicated a statistically significant association between increased Psf3 expression and lower overall survival rate (hazard ratio, 5.2; $P=0.0027$). In a subgroup analysis of only stage I patients, increased Psf3 expression was also significantly associated with a lower overall survival rate ($P=0.0008$, log-rank test). Moreover, the Ki67 index level was higher in the Psf3-positive group than in the Psf3-low positive group ($P<0.0001$, Mann–Whitney U-test). Our results indicated that Psf3 can serve as a prognostic biomarker in lung adenocarcinoma.

1. Introduction

Psf3 is a member of the evolutionarily conserved heterotetrameric complex GINS comprising Sld5, Psf1, Psf2, and Psf3. GINS was originally identified in *Saccharomyces cerevisiae*, and its *Xenopus laevis* homolog has been characterized in egg extracts [1–3]. In *Eukarya*, the GINS complex associates with the mini-chromosome maintenance (MCM) proteins Mcm2–7 and with Cdc45 to form the Cdc45, Mcm2–7, GINS (CMG) complex, which in turn regulates both the initiation and the progression of DNA replication [4–7]. The CMG complex constitutes the eukaryotic replicative DNA helicase and contributes to the recruitment of the replicative polymerases essential for the synthesis of leading and lagging strands [7–10]. While the GINS components that play a part in the initiation of DNA replication seem to have an important role in the accelerated DNA replication of cancer cells, the oncological significance of them is not yet clear.

Several recent reports have suggested that Psf1 is required for the acute proliferation of cells, particularly immature cells such as stem cells and progenitor cells and that this protein is useful in the successful detection of cancer stem cells [11–14]. Moreover, previous studies have suggested that some GINS complex members are upregulated in cancer, and some GINS components may be useful in the detection of cancer stem cells.

Although several studies have suggested that GINS components play a role in cancer [15–18], the expression status of these components in lung adenocarcinoma has not yet been examined. Therefore, we sought to evaluate the expression status of Psf3 by immunohistochemical examination of surgically resected samples of human primary lung adenocarcinoma tissue. We also investigated whether Psf3 expression in tumor tissues influenced the outcome of these patients.

2. Materials and methods

2.1. Patients

The study population comprised 125 consecutive patients (71 males, 54 females) who were examined and treated at Kobe

* Corresponding author. Tel.: +81 78 382 5942; fax: +81 78 382 5959.
E-mail address: maniwa@med.kobe-u.ac.jp (Y. Maniwa).

0169-5002/$ – see front matter © 2012 Elsevier Ireland Ltd. All rights reserved.
http://dx.doi.org/10.1016/j.lungcan.2012.10.001

Table 1
Association between increased expression of Psf3 and clinicopathological characteristics in 125 patients with lung adenocarcinoma.

Variable	Total	Psf3		*P*-value
		Low positive	Positive	
No. patients (%)	125	98	27	NA
Age in years, mean ± SD (range)	67.4 ± 8.8 (42–84)	67.6 ± 8.6 (42–84)	66.5 ± 9.6 (42–81)	0.573
Gender				
Male/female	71/54	55/43	16/11	0.770
T factor				
T1/T2/T3/T4	69/42/4/10	60/29/1/8	9/13/3/2	0.0077*
N factor				
N0/N1/N2/N3	87/13/24/1	76/8/14/0	11/5/10/1	0.0013*
M factor				
M0/M1	122/3	97/1	25/2	0.226
Stage				
I/II/III/IV	82/12/28/3	73/7/17/1	9/5/11/2	0.0004*
P factor				
0/1/2/3	86/19/12/8	72/17/7/2	14/2/5/6	0.0003*
PA invasion				
Negative/positive	101/24	82/16	19/8	0.120
PV invasion				
Negative/positive	74/51	64/34	10/17	0.008*
LY invasion				
Negative/positive	75/50	64/34	11/16	0.021*

LY, lymphatic duct; NA, not applicable; PA, pulmonary artery; PV, pulmonary vein.
* Significant *P*-value.

University Hospital between 2001 and 2004 for lung adenocarcinoma. All cases underwent complete resection in this study. Of the 125 patients, 55, 27, eight, four, 23, five and three had stage IA, IB, IIA, IIB, IIIA, IIIB and IV tumors, respectively (Table 1). Of the N2/N3 patients, three, one and eight patients received induction chemotherapy, radiation and chemoradiotherapy, respectively. Four patients were administered postoperative adjuvant chemotherapy. The study protocol was approved by the Regional Ethics Committee for Clinical Research of Kobe University, and the study was conducted according to the principles of the Declaration of Helsinki. All patients provided written informed consent. Details of the clinical and demographic information, prognostic factors, and disease progression were collected retrospectively.

2.2. Immunohistochemistry

Formalin-fixed, paraffin-embedded specimens were cut at the maximal area of tumor mass into 5-μm-thick slices, and the sections were deparaffinized with xylene and rehydrated with ethanol. For antigen retrieval, the specimens were placed in Dako REAL-Target Retrieval Solution (Dako, Glostrup, Denmark) at 98 °C for 20 min. Mouse anti-human Psf3 monoclonal antibodies (1:500; GeneStem Co., Ltd., Osaka, Japan) were used as the primary antibodies for the detection of Psf3. The Dako LSAB2 Universal (DAB) kit (Dako) was used for endogenous peroxidase blocking, treatment with a secondary antibody against anti-mouse and anti-rat immunoglobulin antibody, and the visualization of HRP. Hematoxylin staining was used as the counterstain. Photographs of the stained sections were obtained using a camera mounted on a Keyence BZ-8000 digital microscope (Keyence, Osaka, Japan).

2.3. Classification of immunohistochemical staining patterns

Immunochemically stained sections were classified by light microscopy. Because Psf3 is a nuclear protein, only sharply defined areas of HRP staining in the nuclei were judged as Psf3 staining. If HRP staining was observed in other structures, such as the cytoplasm, it was judged as background staining. Psf3 localized and functioned only in the nuclei in the previous reports and any specific staining of Psf3 in the cytoplasm was not detected in this study. This assessment method ensured objective and reproducible measurement. The ratio of the cells positive for nuclear staining in a given microscopic field (×200) was determined for each tissue sample, and the expression status was assessed on the basis of this ratio. The status of Psf3 expression as follows: if more than 50% of cancer cells in any microscopic field (×200) of tumor tissues showed nuclear staining, the tissues were considered Psf3 positive; if the ratio of positive nuclear staining was lower than 50% for all the examined microscopic fields, the tissue was deemed Psf3 low positive.

2.4. Statistical analysis

Associations between Psf3 expression on cancer cells and clinicopathological features were determined using the χ^2-test. Survival was examined using the Kaplan–Meier method, and the significance of the difference was evaluated by a log-rank test. Variable effects on survival time were investigated using Cox's regression model. Statistical analysis was performed using the software JMP version 8 (SAS Institute, Cary, NC, USA). A threshold level of 0.05 was set for statistical evaluation.

3. Results

3.1. Psf3 expression in cancer cells of human lung adenocarcinoma

The expression status of Psf3 was determined in 125 lung adenocarcinomas and the adjacent normal lung tissues by immunohistochemistry (IHC), with the use of anti-human Psf3 monoclonal antibodies. In normal lung tissues, Psf3 expression was not detected (Fig. 1A). In some tumor tissues, the nuclei of cancer cells were stained in a scattered pattern, and the ratio of the Psf3-positive cells was less than 10% (Fig. 1B). In contrast, some tissues showed stained nuclei clustered in some areas of tumor tissues, and the ratio of stained cells in such tissue samples was more than 80% (Fig. 1C). These tissue samples showing clustered nuclear staining were classified as Psf3 positive. Thus, we determined the status of Psf3 expression as follows: if more than 50% of cancer cells in any microscopic field (×200) of tumor tissues showed nuclear staining, the tissues were considered Psf3 positive; if the ratio of positive nuclear staining was lower than 50% for all the examined

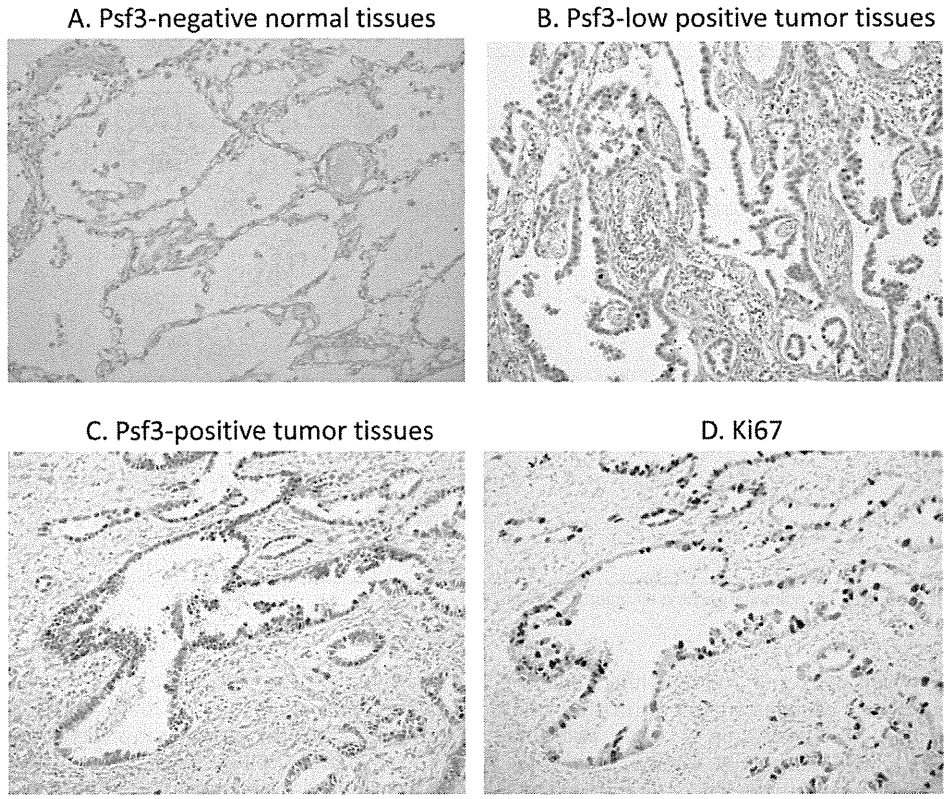

Fig. 1. An immunohistochemical analysis of the Psf3 expression status in cancer cells of human primary lung adenocarcinoma is illustrated. (A) Psf3-negative normal lung tissues. The staining of nuclei was not detected in epithelial or interstitial tissue. (B) Psf3-low positive tumor tissues. The nuclei of cancer cells were stained in a scattered pattern. The ratio of the positive cells was less than 10% (C) Psf3-positive tumor tissues. The stained nuclei were clustered at some regions of the tumor tissues. The ratio of the stained cells in these areas was more than 80%. (D) Immunohistochemical analysis of the expressions of Psf3 and Ki67 in serial sections. While almost all nuclei of the cancer cells were stained with the Psf3 antibody, Ki67 staining was observed in a scattered pattern in the same areas. Ki67 index; 40%.

microscopic fields, the tissue was deemed Psf3 low positive. Of the specimens examined, 98 (78.4%) were low positive for Psf3, while 27 (21.6%) were positive for Psf3 expression.

3.2. Relationship between Psf3 expression and clinicopathological characteristics of patients

In order to evaluate the role of Psf3 in lung adenocarcinoma, we investigated whether Psf3 expression was associated with any of clinicopathological variables in the 125 enrolled cases of primary lung adenocarcinoma (Table 1). The results of the analysis revealed that Psf3 expression was significantly associated with T factor ($P=0.0077$), TNM stage ($P=0.0004$), P factor ($P=0.0003$), lymph node metastasis ($P=0.02$), invasion of the pulmonary vein ($P=0.008$), and cancer cell invasion of the lymphatic ducts ($P=0.02$). No significant relationship was noted between Psf3 expression and age ($P=0.57$), gender ($P=0.77$), distant metastasis ($P=0.22$), and cancer spread to the pulmonary artery ($P=0.12$). These results suggest that increased Psf3 expression may enhance cancer cell proliferation and tumor progression, thereby resulting in the spread of cancer cells into the tumor vessels.

3.3. Increased expression of Psf3 was related to poor patient prognosis

Using the data collected from 125 study patients, we evaluated their prognosis and its relationship to the expression of Psf3. Follow-up data of all the 125 cases were available, for at least 5 years after surgery. We examined the overall survival (OS) of Psf3-low positive and Psf3-positive groups and found a statistically significant difference between the 2 groups by using the log-rank test ($P<0.0001$). The survival of Psf3-low positive patients was greater than that of the Psf3-positive patients (Fig. 2A). A univariate analysis indicated that among the clinicopathological factors, gender (male), tumor classification, lymph node metastasis, invasion of the pulmonary vein, and increased Psf3 expression correlated with the outcome (Table 2). Further assessment using the Cox multivariate analysis indicated that gender (male), lymph node metastasis, and increased Psf3 expression were statistically significant predictors for poor OS (Table 2).

3.4. Increased expression of Psf3 was also related to poor patient prognosis in stage I lung adenocarcinoma

In the current study, we analyzed the association of clustered Psf3 expression in stage I lung adenocarcinoma. Among the stage I cases, 9 (11.0%) and 73 (89.0%) patients were classified as Psf3 positive and Psf3 low positive, respectively (Table 1). A survival analysis that included only stage I patients revealed that the OS curve for the Psf3-positive group was lower than that for the Psf3-low positive group. The log-rank test showed that the intergroup difference was statistically significant ($P=0.0008$; Fig. 2B).

3.5. Relationship between Psf3 expression and Ki67 index

We examined the relationship between increased Psf3 expression and cancer cell proliferation. We used the Ki67 (MIB-1) expression index as an indicator of cell proliferation. In this study, the Ki67 index was calculated using the maximal section of the tumor mass. Using the Mann–Whitney *U*-test, the Ki67 index level

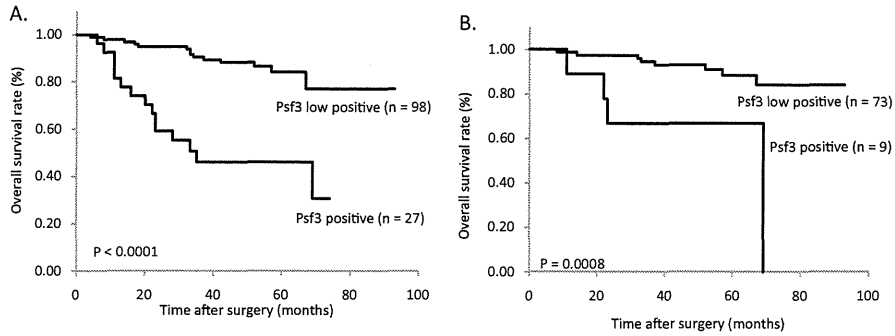

Fig. 2. (A) Kaplan–Meier plot of the overall survival rate in 125 patients with lung adenocarcinoma and its relationship to the Psf3 expression status. *P*-value was determined using the log-rank test. (B) Kaplan–Meier plot of the overall survival rate in 82 patients with lung adenocarcinoma and its relationship to the Psf3 expression status in stage I patients. *P*-value was determined using the log-rank test.

Table 2
Univariate and multivariate analyses of the association between the overall survival of 125 patients with lung adenocarcinoma and prognostic factors by Cox proportional hazard models.

Variable	Hazard ratio	95% confidence interval	*P*-value
Univariate			
Age	1.01	0.96–1.06	0.621
Gender (male versus female)	3.21	1.26–8.20	0.014*
T factor (T1<)	3.27	1.38–7.78	0.0071*
LN (negative versus positive)	5.62	2.32–13.5	0.0001*
PV invasion (negative versus positive)	3.40	1.44–8.00	0.0051*
Psf3 (low positive versus positive)	6.91	2.70–17.6	0.0001*
Multivariate			
Age	1.03	0.97–1.09	0.260
Gender(male versus female)	4.27	1.36–13.4	0.012*
T factor (T1<)	2.30	0.78–6.75	0.129
LN (negative versus positive)	4.08	1.32–12.5	0.014*
PV invasion (negative versus positive)	0.92	0.29–2.88	0.886
Psf3 (low positive versus positive)	5.22	1.77–15.3	0.0027*

LN, lymph node metastasis; PV, invasion of the pulmonary vein.
* Significant *P*-value.

was found to be higher in the Psf3-positive group than in the Psf3-low positive group. The median Ki67 index was 5% and 17% in the Psf3-low positive and Psf3-positive tumors, respectively (Fig. 3).

Additionally, immunochemical staining of Ki67 was also performed on serial sections that were used for Psf3 staining. The ratio of Ki67-positive cancer cells was found to be higher in areas where excessive staining of the nuclei of cancer cells was observed when tested with the Psf3 antibody (Fig. 1C and D). However, different staining patterns were observed for Ki67 and Psf3. While almost all nuclei of cancer cells were stained with the Psf3 antibody in the clustered area (Fig. 1C), Ki67 staining was observed in a scattered pattern, and the ratio of Ki67-positive nuclei was less than 50% (Fig. 1D).

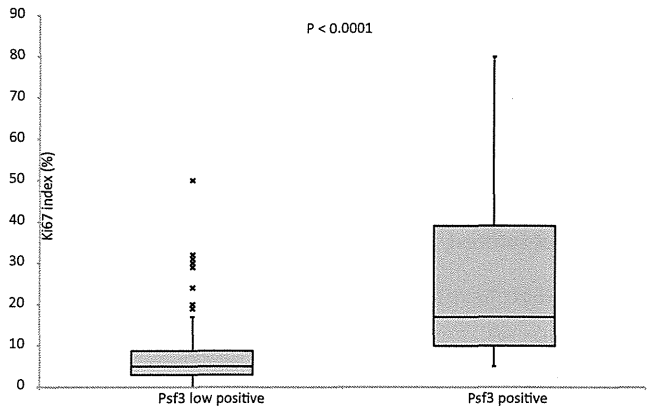

Fig. 3. Ki67 index (%) in lung adenocarcinoma samples and its relationship to the Psf3 expression status. *P*-value was determined using the Mann–Whitney *U*-test.

3.6. *Psf3: most powerful predictor of poor prognosis in lung adenocarcinoma patients*

We have previously performed IHC for 10 cancer-related proteins (CDC45, HIF1, sirt1, E-cadhelin, Nectin3, and the proteins listed in Table 3 other than Psf3) with the same paraffin-embedded specimens of the 125 cases investigated in this study [19,20] and examined the relationship between their expression in cancer cells and the prognosis of the patients. Univariate analysis revealed the significant association of 5 of the proteins with poor prognosis. To clarify the prognostic value of Psf3 expression in cancer cells, we statistically compared the expression levels of these 5 proteins and Psf3. Multivariate analysis revealed that Psf3 was the strongest predictor of poor prognosis (Table 3).

4. Discussion

Psf3 is a member of the GINS complex, along with Sld5, Psf1, and Psf2. Psf1 is tightly regulated at the transcriptional level in stem cells and enables the successful detection of cancer stem cells [11–14]. Therefore, it seems reasonable that other GINS components may also facilitate the detection of cancer stem cells in tumors. Cancer stem cells, which are resistant to anti-cancer drugs and irradiation, appear to be responsible for tumor growth in hematological and solid cancers. The detection of these cells is critical for identifying molecular targets to inhibit their growth. We conducted

this study on the basis of the hypothesis that Psf3 may also be a marker for cancer stem cells. Previous study has shown that all GINS components overexpression in intrahepatic cholangiocarcinoma tissues and Psf3 expression in human colon carcinoma [15,17]. To our knowledge, this is the first study to detect Psf3 expression in lung adenocarcinoma and to show that Psf3 expression might be a useful prognostic marker for assessing patient survival in lung adenocarcinoma.

In this study, we performed IHC of surgically resected lung adenocarcinoma specimens to determine the Psf3 status in cancer cells and cancer tissues clinically. The results of IHC revealed that the protein was specifically localized to the nuclei of cancer cells. The staining pattern for Psf3 was quite characteristic and reproducible.

IHC revealed that Psf3 expression was increased in 21.6% (27/125) of the lung adenocarcinoma specimens but not in normal lung tissues (Fig. 1A). In order to elucidate the role of increased Psf3 expression on the prognosis of patients with lung adenocarcinoma, a prognostic analysis was carried using the patients' follow-up data. Survival analysis revealed that the OS rate in patients positive for increased Psf3 expression was notably lower than that of the Psf3-low positive group (Fig. 2A). These findings indicated that increased Psf3 expression low positively affected the clinical course and was correlated with malignant behavior of tumors. The significance of Psf3 expression in cancer cells on these clinical features was also supported by our analysis of the relationship between Psf3 expression and clinicopathological characteristics of 125 patients (Table 2). Cox multivariate analysis indicated that increased Psf3 expression was the most significant predictor of poor prognosis, rather than the pathological T factor or N factor. Furthermore, a prognostic analysis that included only stage I cases revealed that the OS rate of the Psf3-positive group was significantly lower than that of the Psf3-low positive group. These findings suggest that increased Psf3 expression may be used as a reference index for molecular staging of patients with a high risk of death and thereby likely to benefit from intensive adjuvant therapy.

What is the basis of the relationship between increased Psf3 expression and poor prognosis? We believe that increased Psf3 expression may be related to cancer cell proliferation because Psf3 was required in the early stage of DNA replication, along with other GINS members [11–14]. In this study, Ki67 (MIB-1) expression index was used as an indicator of cell proliferation. The Mann–Whitney *U*-test indicated that the Ki67 index level was higher in the Psf3-positive group than in the Psf3-low positive group (Fig. 3).

Table 3
Univariate and multivariate analysis of the association between the overall survival of 125 patients with lung adenocarcinoma and other candidates for biomarkers by Cox proportional hazard models.

Variable	Hazard ratio	95% confidence interval	*P*-value
Univariate			
Ki67	1.02	1.00–1.05	0.0412*
γ-H2AX	1.73	0.75–4.00	0.193
p53	1.17	0.51–2.69	0.699
Necl-5	1.82	0.49–6.74	0.368
Wip1	7.32	1.56–34.2	0.0113*
Psf3	6.91	2.70–17.6	0.0001*
Multivariate			
Ki67	0.97	0.93–1.01	0.266
γ-H2AX	0.77	0.22–2.73	0.695
p53	0.80	0.23–2.73	0.726
Necl-5	1.42	0.25–7.95	0.688
Wip1	4.77	0.89–25.5	0.067
Psf3	12.1	2.51–58.3	0.0019*

γ-H2AX, phosphorylated H2AX; p53, tumor protein p53; Necl-5, Nectin-like molecule-5; Wip1, Wild-type p53-induced phosphatase 1.
* Significant *P*-value.

Subsequently, we examined the status of cell proliferation at the Psf3-positive sites in cancer tissues in order to investigate the role of Psf3 expression on cancer cell biology, by using serial sections of cancer tissues. The ratio of Ki67-positive cancer cells was extremely higher in areas with excessive nuclear staining of Psf3 (Fig. 1C and D). This finding indicated that the proliferation potential was specifically higher at these areas. The accumulation of Psf3 in the nuclei of the cancer cells might be indicative of its role in the acceleration of cancer cell proliferation.

Additionally, we compared the staining patterns of Ki67 and Psf3 in the same serial sections and found that the staining patterns of the 2 proteins were different. While almost all nuclei of cancer cells were stained with the Psf3 antibody in the clustered area (Fig. 1C), Ki67 staining was observed in a "scattered pattern" and the ratio of Ki67-positive nuclei was ≤50% (Fig. 1D). During the cell cycle of eukaryotic cells, Ki67 is expressed at increased levels during the S phase, with the maximum expression in the M phase [21,22]. In other words, the cells with nuclear staining for Ki67 antibody are in the middle of cell division. Thus, the staining pattern ("scattered pattern") of Ki67 detected in our study is consistent with the biological role of Ki67. Because cancer cells in each phase are randomly distributed in cancer tissues and Ki67 level in nuclei was functionally increasing and decreasing in cell cycle dependent manner, the "scattered" pattern of Ki67 staining was observed.

On the other hand, staining for Psf3 showed a pattern different from that of staining for Ki67. In some tumor tissues, the nuclei of cancer cell were stained in a "scattered pattern" (judged as low positive for Psf3 in this study) similar to that observed for Ki67. In other cases, clustered nuclear staining (judged as positive for Psf3 in this study) was observed in some areas of tumor tissues. These findings were suggestive of the aberrant accumulation of Psf3 in the nuclei of the clustered area. While Psf3 staining in a "scattered pattern" seemed to be dependent on the cell cycle, similar to the case with Ki67, the clustered pattern of staining for Psf3 was persistently observed in nuclei of cancer cells out of the cell cycle.

We previously performed IHC analysis of 10 cancer-related proteins by using the same paraffin-embedded specimens examined in this study and compared the expression levels of these proteins and Psf3 to determine the strongest predictor of poor prognosis. Statistical analysis revealed that Psf3 was the most promising candidate as a marker of poor prognosis (Table 3). Immunohistochemical investigation of Psf3 expression in lung cancer specimens seems to be a useful tool because of the following reasons: (1) its statistically significant association with poor prognosis, (2) the objectivity and reproducibility of the test for positive expression because of the specific and sharply defined staining pattern, and (3) the existence of biological and pathological evidence regarding Psf3.

In conclusion, our results suggested that increased Psf3 expression in cancer cells in primary lung adenocarcinoma plays an important role in the progression of lung adenocarcinoma and acts as a factor low positively affecting the prognosis of patients. These results suggested that Psf3 could be used as a reference index for the molecular staging to select patients at high risk of death and relapsed patients who may benefit from intensive adjuvant therapy.

Conflicts of interest

The authors have no conflicts of interest to declare.

Acknowledgments

This study was supported by grant 23592060 from the Japan Society for the Promotion of Science (to Y.M.) and 23-A-18 from

the National Cancer Center Research and Development Fund (to M.Y.).

References

[1] Takayama Y, Kamimura Y, Okawa M, Muramatsu S, Sugino A, Araki H. GINS, a novel multiprotein complex required for chromosomal DNA replication in budding yeast. Genes Dev 2003;17:1153–65.
[2] Kanemaki M, Sanchez-Diaz A, Gambus A, Labib K. Functional proteomic identification of DNA replication proteins by induced proteolysis in vivo. Nature 2003;423:720–4.
[3] Kubota Y, Takase Y, Komori Y, Hashimoto Y, Arata T, Kamimura Y, et al. A novel ring-like complex of Xenopus proteins essential for the initiation of DNA replication. Genes Dev 2003;17:1141–52.
[4] Moyer SE, Lewis PW, Botchan M. Isolation of the Cdc45/Mcm2-7/GINS (CMG) complex, a candidate for the eukaryotic DNA replication fork helicase. Proc Natl Acad Sci USA 2006;103:10236–41.
[5] Gambus A, Jones RC, Sanchez-Diaz A, Kanemaki M, van Deursen F, Edmondson RD, et al. GINS maintains association of Cdc45 with MCM in replisome progression complexes at eukaryotic DNA replication forks. Nat Cell Biol 2006;8:358–66.
[6] Pacek M, Tutter AV, Kubota Y, Takisawa H, Walter JC. Localization of MCM2–7, Cdc45, and GINS to the site of DNA unwinding during eukaryotic DNA replication. Mol Cell 2006;21:581–7.
[7] Bermudez V, Farina A, Raghavan V, Tappin I, Hurwitz J. Studies on human DNA polymerase epsilon and GINS complex and their role in DNA replication. J Biol Chem 2011;286:28963–77.
[8] Kang YH, Galal WC, Farina A, Tappin I, Hurwitz J. Properties of the human Cdc45/Mcm2-7/GINS helicase complex and its action with DNA polymerase epsilon in rolling circle DNA synthesis. Proc Natl Acad Sci USA 2012;109:6042–7.
[9] Kamada K, Kubota Y, Arata T, Shindo Y, Hanaoka F. Structure of the human GINS complex and its assembly and functional interface in replication initiation. Nat Struct Mol Biol 2007;14:388–96.
[10] De Falco M, Ferrari E, De Felice M, Rossi M, Hubscher U, Pisani FM. The human GINS complex binds to and specifically stimulates human DNA polymerase alpha-primase. EMBO Rep 2007;8:99–103.
[11] Ueno M, Itoh M, Kong L, Sugihara K, Asano M, Takakura N. Psf1 is essential for early embryogenesis in mice. Mol Cell Biol 2005;25:10528–32.
[12] Ueno M, Itoh M, Sugihara K, Asano M, Takakura N. Both alleles of Psf1 are required for maintenance of pool size of immature hematopoietic cells and acute bone marrow regeneration. Blood 2009;113:555–62.
[13] Han Y, Ueno M, Nagahama Y, Takakura N. Identification and characterization of stem cell-specific transcription of Psf1 in spermatogenesis. Biochem Biophys Res Commun 2009;280:609–13.
[14] Nagahama Y, Ueno M, Miyamoto S, Morii E, Minami T, Mochizuki N, et al. Psf1, a DNA replication factor expressed widely in stem and progenitor cells, drives tumorigenic and metastatic properties. Cancer Res 2010;70:1215–24.
[15] Obama K, Ura K, Satoh S, Nakamura Y, Furukawa Y. Up-regulation of Psf2, a member of the GINS multiprotein complex, in intrahepatic cholangiocarcinoma. Oncol Rep 2005;14:701–6.
[16] Ryu B, Kim DS, Deluca AM, Alani RM. Comprehensive expression profiling of tumor cell lines identifies molecular signatures of melanoma progression. PLoS ONE 2007;2:e594.
[17] Nagahama Y, Ueno M, Haraguchi N, Mori M, Takakura N. Psf3 marks malignant colon cancer and has a role in cancer cell proliferation. Biochem Biophys Res Commun 2010;5:150–4.
[18] Nakahara I, Miyamoto M, Shibata T, Akashi-Tanaka S, Kinoshita T, Mogushi K, et al. Up-regulation of Psf1 promotes the growth of breast cancer cells. Genes Cells 2010;15:1015–24.
[19] Satoh N, Maniwa Y, Bermudez VP, Nishimura K, Nishio W, Yoshimura M, et al. Oncogenic phosphatase Wip1 is a novel prognostic marker for lung adenocarcinoma patient survival. Cancer Sci 2011;102:1101–6.
[20] Nakai R, Maniwa Y, Tanaka Y, Nishio W, Yoshimura M, Okita Y, et al. Overexpression of Necl-5 correlates with unfavorable prognosis in patients with lung adenocarcinoma. Cancer Sci 2010;101:1326–30.
[21] Scholzen T, Gerdes J. The Ki-67 protein: from the known and the unknown. J Cell Physiol 2000;182:311–22.
[22] Landberg G, Tan EM, Roos G. Flow cytometric multiparameter analysis of proliferating cell nuclear antigen/cyclin and Ki-67 antigen: a new view of the cell cycle. Exp Cell Res 1990;187:111–8.

Solid tumors versus mixed tumors with a ground-glass opacity component in patients with clinical stage IA lung adenocarcinoma: Prognostic comparison using high-resolution computed tomography findings

Yasuhiro Tsutani, MD, PhD,[a] Yoshihiro Miyata, MD, PhD,[a] Takeharu Yamanaka, PhD,[b] Haruhiko Nakayama, MD, PhD,[c] Sakae Okumura, MD, PhD,[d] Shuji Adachi, MD, PhD,[e] Masahiro Yoshimura, MD, PhD,[f] and Morihito Okada, MD, PhD[a]

Objective: This study aimed to compare malignant behavior and prognosis between solid tumors and mixed tumors with a ground-glass opacity component on high-resolution computed tomography.

Methods: We examined 436 of 502 consecutive patients with clinical stage IA adenocarcinoma who had undergone preoperative high-resolution computed tomography and F-18-fluorodeoxyglucose positron emission tomography/computed tomography; 66 patients with tumors with pure ground-glass opacity components were excluded. Tumor type (solid, n = 137; mixed, n = 299) and surgical results were analyzed for all patients and their matched pairs.

Results: In all patients, solid tumors showed a significantly greater association ($P < .001$) with lymphatic, vascular, and pleural invasion and lymph node metastasis compared with mixed tumors. The disease-free survival was also worse in patients with solid tumors ($P = .0006$). Analysis of 97 pairs matched for solid component size confirmed that solid tumors were significantly associated with lymphatic, vascular, and pleural invasion ($P = .008$, $P = .029$, $P = .003$, respectively) and poor prognosis. When maximum standardized uptake value and solid component size were matched (n = 79), the differences in pathologic prognostic parameters and disease-free survivals between patients with solid and mixed tumors disappeared.

Conclusions: Solid tumors exhibit more malignant behavior and have a poorer prognosis compared with mixed tumors, even when the solid component size is the same in both tumor types. However, differences in malignant behavior can be identified using maximum standardized uptake values determined by F-18-fluorodeoxyglucose positron emission tomography/computed tomography. (J Thorac Cardiovasc Surg 2013;146:17-23)

The recent development of high-resolution computed tomography (HRCT) and low-dose computed tomography (CT) screening has improved the detection of small lung cancers, especially lung adenocarcinomas.[1-3] These often contain a nonsolid component that presents as a ground-glass opacity (GGO) on HRCT and is closely associated with bronchioloalveolar carcinoma.[4,5] We have previously reported the benefits of comparing solid component size (the maximum dimension of the solid component excluding GGO) on HRCT with whole tumor size for predicting the pathologic invasiveness of tumors or the prognosis of clinical stage IA lung adenocarcinomas.[6] It remains unclear whether GGO-containing tumors have the same malignant behavior and prognosis as pure solid tumors after matching for solid component size.

Whether or not differences exist in malignant behavior between pure solid tumors and mixed tumors with a GGO component on HRCT remains controversial. Therefore, we used HRCT to compare malignant behavior, including lymphatic, vascular, and pleural invasion, and prognosis between solid tumors and mixed tumors having a GGO component in patients with clinical stage IA lung adenocarcinoma.

PATIENTS AND METHODS

Between August 1, 2005, and December 31, 2009, we enrolled 502 patients with clinical T1N0M0 stage IA lung adenocarcinoma who were admitted to 1 of the following 4 institutions: Hiroshima University, Kanagawa Cancer Center, Cancer Institute Hospital, and Hyogo Cancer Center. HRCT and F-18-fluorodeoxyglucose positron emission tomography/CT

From the Department of Surgical Oncology,[a] Hiroshima University, Hiroshima, Japan; Research Center for Innovative Oncology,[b] National Cancer Center Hospital East, Kashiwa, Japan; Department of Thoracic Surgery,[c] Kanagawa Cancer Center, Yokohama, Japan; Department of Thoracic Surgery,[d] Cancer Institute Hospital, Tokyo, Japan; and Departments of Radiology[e] and Thoracic Surgery,[f] Hyogo Cancer Center, Akashi, Japan.

Disclosures: Authors have nothing to disclose with regard to commercial support.
Received for publication Jan 23, 2012; revisions received Sept 14, 2012; accepted for publication Nov 6, 2012; available ahead of print Dec 14, 2012.

Address for reprints: Morihito Okada, MD, PhD, Department of Surgical Oncology, Research Institute for Radiation Biology and Medicine, Hiroshima University, 1-2-3-Kasumi, Minami-ku, Hiroshima City, Hiroshima 734-0037, Japan (E-mail: morihito@hiroshima-u.ac.jp).

0022-5223/$36.00

http://dx.doi.org/10.1016/j.jtcvs.2012.11.019

GTS

Abbreviations and Acronyms

CT = computed tomography
DFS = disease-free survival
FDG-PET = F-18-fluorodeoxyglucose positron emission tomography
FOV = field of view
GGO = ground-glass opacity
HRCT = high-resolution computed tomography
SUV = standardized uptake value
SUVmax = maximum standardized uptake value

(FDG-PET/CT) followed by curative R0 resection were performed in all patients, who were staged according to the seventh edition of the TNM classification of malignant tumors.[7] Mediastinoscopy and endobronchial ultrasonography were not routinely performed because HRCT revealed no swelling of mediastinal or hilar lymph nodes and FDG-PET showed no accumulation in these lymph nodes in all patients. Sublobar resections (segmentectomy or wedge resection) were performed if the tumor mainly comprised a GGO component or had no lymph node metastasis on intraoperative assessment. Tumors with pure GGO were excluded from the analyses because they are noninvasive and have an extremely good prognosis.[8,9] We obtained appropriate approval for this multicenter study from the institutional review board of each institution, which waived the requirement for informed consent from individual patients because this was a retrospective review of medical records from a prospective database.

High-Resolution Computed Tomography

Chest images were obtained using 16-row multidetector CT independently of subsequent FDG-PET/CT examinations. High-resolution images of the tumors were acquired using the following parameters: 120 kVp; 200 mA; section thickness, 1 to 2 mm; pixel resolution, 512 × 512; scanning time, 0.5 to 1 seconds; a high spatial reconstruction algorithm with a 20-cm field of view (FOV); and mediastinal (level, 40 HU; width, 400 HU) and lung (level, −600 HU; width, 1600 HU) window settings. GGO was defined as a misty increase in lung attenuation that did not obscure underlying vascular markings. We defined solid component size as the maximum dimension of the solid component in the lung windows after excluding the GGO component.[6] Solid tumors were defined as pure solid tumors without a GGO component, whereas mixed tumors were defined as tumors with a GGO component regardless of the GGO proportion.

F-18-Fluorodeoxyglucose Positron Emission Tomography/Computed Tomography

Patients were instructed to fast for more than 4 hours before intravenous injection of 74 to 370 MBq of FDG. After injection, they were instructed to relax for at least 1 hour before FDG-PET/CT scanning. Blood glucose was calculated before tracer injection to confirm a level of less than 150 mg/dL.[10] Patients with blood glucose values 150 mg/dL or greater were excluded from PET/CT image acquisition. Images were obtained using Discovery ST (GE Healthcare, Little Chalfont, UK), Aquiduo (Toshiba Medical Systems Corporation, Tochigi, Japan), or Biograph Sensation16 (Siemens Healthcare, Erlangen, Germany) integrated PET/CT scanners. Low-dose, unenhanced CT images of 2- to 4-mm section thickness for attenuation correction and localization of lesions identified by PET were obtained from the head to the pelvic floor of each patient using a standard protocol. Immediately after CT, PET covered the identical axial FOV for 2 to 4 minutes per table position depending on the condition of the patient and scanner performance. All PET images with a 50-cm FOV were reconstructed using an iterative algorithm with CT-derived attenuation correction. Variations in standardized uptake values (SUVs) among institutions were minimized using an anthropomorphic body phantom. A calibration factor was obtained by dividing the actual SUV by the gauged mean SUV in the phantom background to decrease interinstitutional SUV inconsistencies; the final SUV used is referred to as the revised maximum SUV (SUVmax).[11,12] Adjustment of interinstitutional variability in SUV narrowed the range from 0.89 to 1.24 to 0.97 to 1.18 when the SUVmax ratio was expressed as the SUVmax reported by each institute relative to the SUVmax reported by the control institute.

Follow-up Evaluation

All patients who underwent lung resection were followed up from the day of surgery. Postoperative follow-up procedures, including physical examination and chest roentgenography every 3 months and chest and abdominal CT examinations every 6 months, were performed for the first 2 years. Thereafter, physical examination and chest roentgenography were performed every 6 months, whereas chest CT examination was performed every year. Recurrence was determined by radiographic features or histologic evidence.

Statistical Analysis

Data are presented as numbers (%) or mean ± standard deviation unless otherwise stated. Frequencies were compared using the chi-square test for categoric variables, and the Fisher exact test was applied to small samples in all cohort patients. McNemar tests were used for analyses of matched-pair patients. Mann–Whitney U tests and t tests were used to compare continuous variables in all cohort patients. Wilcoxon tests were used for analyses of matched-pair patients. Disease-free survival (DFS) was defined as the time from the date of surgery until the first event (relapse or death from any cause) or last follow-up. The duration of DFS was analyzed using the Kaplan–Meier method. Differences in DFS were assessed using the log-rank test. We applied matching to balance the assignment of the included patients and correct for tumor type (solid or mixed), which confounded survival. The variables were solid component size or SUVmax. Solid and mixed tumor pairs with an equivalent solid component size or SUVmax were selected by a 1-to-1 match. All 436 patients were pooled and sorted in ascending order according to their solid component size or SUVmax. The selection process began from the first 2 cases with the lowest solid component size or SUVmax. If 1 case exhibited a solid tumor and the other case exhibited a mixed tumor, both were selected as a matched pair. If this was not the case, then 4 cases were included. In the same way, solid and mixed tumors were matched by their solid component size or SUVmax in 1:1, 2:2, 3:3, or 4:4 blocks. A patient who did not have a suitable match within the acceptable rank range was excluded from further analysis, and the matching process moved down the sort list until all possible matched pairs were included. The selected patients formed well-matched 1:1 pairs in both groups. Data were analyzed using the Statistical Package for the Social Sciences (v 10.5; SPSS Inc, Chicago, Ill).

RESULTS

Of the 502 patients, 66 who had tumors with pure GGO components were excluded; the remaining 436 patients were included in this analysis. Of the 436 study patients, 137 had solid tumors and 299 had mixed tumors. The mean follow-up period after surgery was 20.2 ± 12.5 months, during which the disease recurred in 29 patients (6.7%). The mean follow-up period was similar for solid and mixed tumors (21.4 ± 12.8 months and 19.7 ± 12.4 months, respectively, $P = .235$). Of the 29 cases of recurrence, 9 (2.1%) were local (including mediastinal lymph node metastasis), 3 (0.7%) were local and distant, and 17

(3.9%) were distant. Age, sex, and whole tumor size on HRCT were not significantly different between patients with solid and mixed tumors. Solid tumors were significantly correlated with a large solid component size, a high SUVmax, and the presence of lymphatic, vascular, and pleural invasion and lymph node metastasis ($P < .001$, $P < .001$, $P < .001$, $P < .001$, $P < .001$, $P = .001$, respectively; Table 1).

Local recurrence occurred in 5 patients (3.6%) with solid tumors (1 involving the bronchial stump and 4 involving the mediastinal lymph nodes) and 4 patients (1.3%) with mixed tumors (1 involving the residual lung after segmentectomy and 3 involving the mediastinal lymph nodes). A significant difference in DFS was identified between patients with solid tumors (n = 137; 2-year DFS, 83.1%) and those with mixed tumors (n = 299; 2-year DFS, 94.2%; $P = .0006$; Figure 1, *A*).

After matching for solid component size, there were 97 well-matched solid and mixed tumor pairs. Significant differences were identified in whole tumor size, SUVmax, and lymphatic, vascular, and pleural invasion between the 2 tumor types ($P < .001$, $P < .001$, $P = .008$, $P = .029$, $P = .003$, respectively, Table 2). Solid tumors were significantly correlated with a small whole tumor size, a high SUVmax, and the presence of pathologic invasiveness.

Furthermore, a difference in DFS was identified between patients with solid tumors (n = 97; 2-year DFS, 83.5%) and those with mixed tumors (n = 97; 2-year DFS, 91.8%; Figure 1, *B*) after matching for solid component size.

TABLE 1. Comparison of solid and mixed tumor characteristics in all cohort patients

	Solid tumors (n = 137)	Mixed tumors (n = 299)	*P*
Age (y)	65.5 ± 10.5	65.7 ± 8.8	.85
Sex			.12
Male	71 (51.8%)	130 (43.5%)	
Female	66 (48.2%)	169 (56.5%)	
Whole tumor size (cm)	2.1 ± 0.6	2.0 ± 0.6	.69
Solid component size (cm)	2.1 ± 0.6	1.1 ± 0.7	<.001
SUVmax	4.9 ± 3.3	2.6 ± 2.9	<.001
Lymphatic invasion			<.001
Negative	89 (65.0%)	270 (90.3%)	
Positive	48 (35.0%)	29 (9.7%)	
Vascular invasion			<.001
Negative	79 (57.7%)	264 (88.3%)	
Positive	58 (42.3%)	35 (11.7%)	
Pleural invasion			<.001
Negative	100 (73.0%)	278 (93.0%)	
Positive	37 (27.0%)	21 (7.0%)	
Lymph node metastasis			<.001
Negative	114 (83.2%)	284 (95.0%)	
Positive	23 (16.8%)	15 (5.0%)	
Procedure			.001
Lobectomy	111 (81.0%)	190 (63.5%)	
Segmentectomy	9 (6.6%)	48 (16.1%)	
Wedge resection	17 (12.4%)	61 (20.4%)	

SUVmax, Maximum standardized uptake value.

After matching for SUVmax, there were 96 well-matched solid and mixed tumor pairs. No significant differences in clinical characteristics, except for solid component size, were found between the 2 tumor types (Table 3).

A difference in DFS was identified between patients with solid tumors (n = 96; 2-year DFS, 87.1%) and those with mixed tumors (n = 96; 2-year DFS, 90.4%; Figure 1, *C*) after matching for SUVmax.

After matching for solid component size and SUVmax, there were 79 well-matched solid and mixed tumor pairs. No significant differences in clinical characteristics, except for whole tumor size, were found between the 2 tumor types (Table 4).

Furthermore, there was no difference in DFS between patients with solid tumors (n = 79; 2-year DFS, 87.0%) and patients with mixed tumors (n = 79; 2-year DFS, 83.9%; Figure 1, *D*) after matching for solid component size and SUVmax.

Figure 2 shows examples of solid and mixed tumors with the same solid component size (1.0 cm). Regardless of tumor type, tumors with low SUVmax were not associated with lymphatic invasion, whereas those with high SUVmax were.

DISCUSSION

The present study demonstrated, as expected, that solid tumors were associated with highly malignant variables, such as large solid component size, high SUVmax, and lymphatic, vascular, and pleural invasion and lymph node metastasis in all cohort patients. In addition, patients with solid tumors had worse DFS than those with mixed tumors. A retrospective study has previously shown that pure solid tumors have malignant potential with nodal or pleural involvement and worse DFS compared with predominantly solid tumors with a GGO component.[13] Other studies have also revealed that tumors with a predominant GGO component are less invasive and have a more favorable prognosis in patients with clinical stage IA lung adenocarcinomas.[4,8,14] Our study is consistent with these findings.

With regard to the tumor size on HRCT, solid component size is more useful than whole tumor size for predicting pathologic invasiveness and prognosis. In our previous study, solid component size was found to have a higher predictive value for lymphatic, vascular, and pleural invasion compared with whole tumor size; furthermore, solid component size was an independent prognostic factor for DFS.[6] It was not clear whether mixed tumors and solid tumors have similar malignant behaviors and prognoses when both have the same solid component size on HRCT. Therefore, we conducted a matched analysis to compare solid and mixed tumors after matching for solid component size in both tumor types. Even after matching for solid component

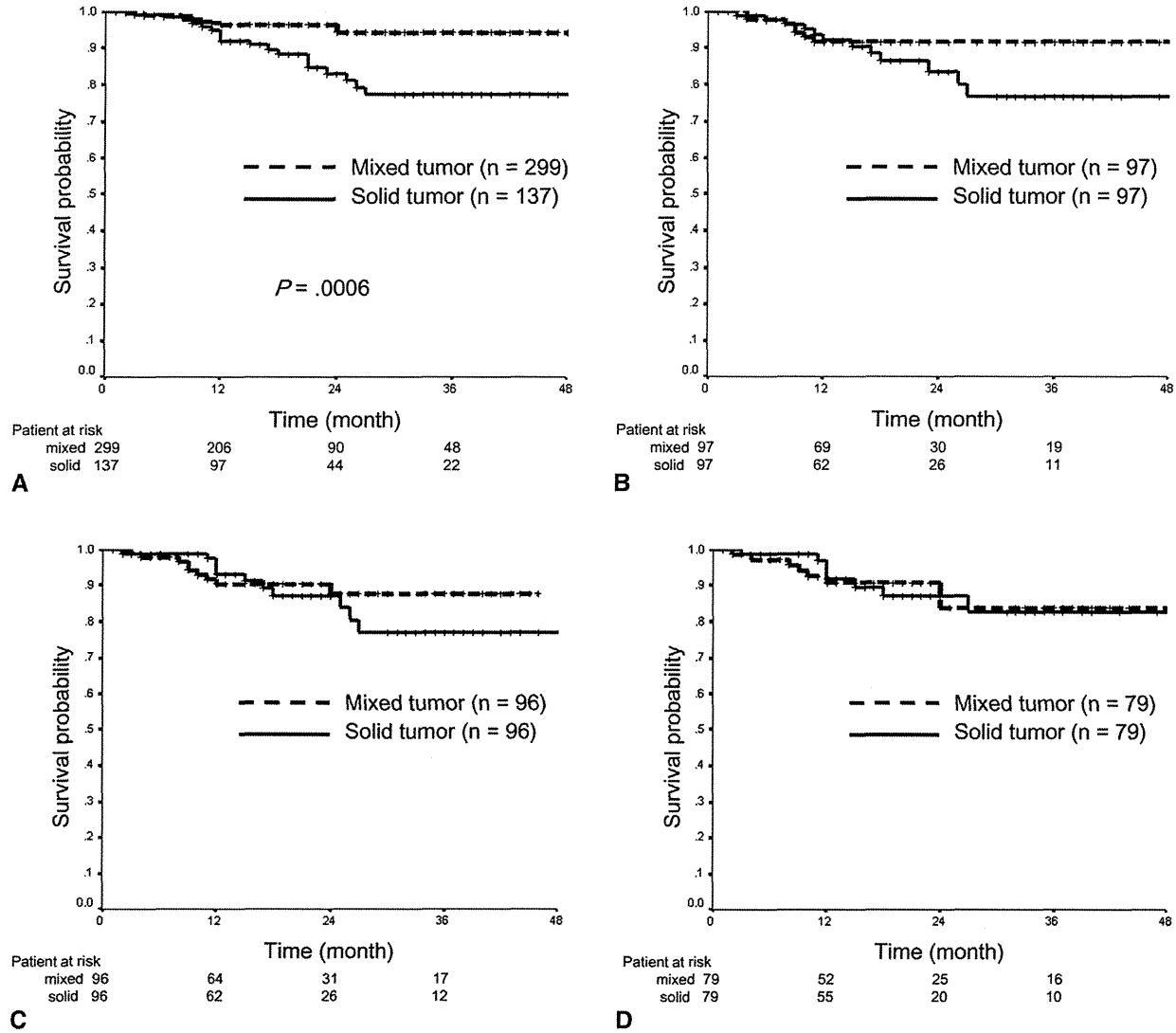

FIGURE 1. DFS curves of patients according to tumor type on HRCT. A, In all cohort patients, 2-year DFS of 94.2% (mean DFS of 47 months; 95% confidence interval [CI], 46-48 months) and 83.1% (mean DFS of 42 months; 95% CI, 39-45 months) were identified for mixed and solid tumors, respectively ($P = .0006$). B, In patients matched for solid component size, 2-year DFS of 91.8% (mean DFS of 46 months; 95% CI, 43-48 months) and 83.5% (mean DFS of 42 months; 95% CI, 38-45 months) were identified for mixed and solid tumors, respectively. C, In patients matched for SUVmax, 2-year DFS of 90.4% (mean DFS of 42 months; 95% CI, 39-44 months) and 87.1% (mean DFS of 42 months; 95% CI, 38-46 months) were detected for mixed and solid tumors, respectively. D, In patients matched for solid component size and SUVmax, 2-year DFS of 83.9% (mean DFS of 43 months; 95% CI, 40-47 months) and 87.0% (mean DFS of 43 months; 95% CI, 40-47 months) were detected for mixed and solid tumors, respectively.

size in both tumor types on HRCT, solid tumors were more frequently correlated with high SUVmax and malignant behavior compared with mixed tumors. In addition, the DFS of patients with solid tumors was worse than that of patients with mixed tumors. This means that solid tumors have more malignant potential than mixed tumors even if both tumor types have the same solid component size on HRCT. This is a new finding. SUVmax on PET/CT is reported to be a predictor of malignant behavior and prognosis in cases of lung adenocarcinomas.[6,11,12,15-17] SUVmax on PET/CT is a preoperative factor, whereas lymphatic, vascular, and pleural invasion are postoperative factors. We have previously reported that SUVmax is a significant predictor of malignant behavior.[6,11,12,16,17]

We experimentally performed a matched analysis to compare solid and mixed tumors after matching for SUVmax. In this matched model, solid tumors and mixed tumors had similar clinical characteristics except solid component size, but there seemed to be a difference in DFS. Although both tumor types have the same SUVmax, solid tumors seem to have a worse potential than mixed tumors.

TABLE 2. Comparison of solid and mixed tumor characteristics in patients matched for solid component size

	Solid tumors (n = 97)	Mixed tumors (n = 97)	*P*
Age (y)	64.9 ± 10.4	66.1 ± 10.0	.63
Sex			.054
Male	50 (51.5%)	36 (37.1%)	
Female	47 (48.5%)	61 (62.9%)	
Whole tumor size (cm)	1.8 ± 0.5	2.3 ± 0.5	<.001
Solid component size (cm)	1.8 ± 0.5	1.8 ± 0.5	N/A
SUVmax	4.8 ± 3.4	3.0 ± 2.5	<.001
Lymphatic invasion			.008
Negative	63 (64.9%)	81 (83.5%)	
Positive	34 (35.1%)	16 (16.5%)	
Vascular invasion			.029
Negative	62 (63.9%)	76 (78.4%)	
Positive	35 (36.1%)	21 (21.6%)	
Pleural invasion			.003
Negative	71 (73.2%)	88 (90.1%)	
Positive	26 (26.8%)	9 (9.9%)	
Lymph node metastasis			.13
Negative	82 (84.5%)	90 (92.8%)	
Positive	15 (15.5%)	7 (7.2%)	
Procedure			.38
Lobectomy	74 (76.3%)	83 (85.6%)	
Segmentectomy	7 (7.2%)	8 (8.2%)	
Wedge resection	16 (16.5%)	6 (6.2%)	

SUVmax, Maximum standardized uptake value; *N/A*, not applicable.

TABLE 3. Comparison of solid and mixed tumor characteristics in patients matched for maximum standardized uptake value

	Solid tumor (n = 96)	Mixed tumor (n = 96)	*P*
Age (y)	65.4 ± 10.4	65.5 ± 9.3	.94
Sex			.26
Male	49	40	
Female	47	56	
Whole tumor size (cm)	2.0 ± 0.6	2.1 ± 0.6	.24
Solid tumor size (cm)	2.0 ± 0.6	1.5 ± 0.7	<.001
SUVmax	4.0 ± 2.6	4.0 ± 2.6	N/A
Lymphatic invasion			.12
Negative	65	74	
Positive	31	22	
Vascular invasion			.47
Negative	62	67	
Positive	34	29	
Pleural invasion			.071
Negative	70	81	
Positive	26	15	
Lymph node metastasis			.54
Negative	80	84	
Positive	16	12	
Procedure			.50
Lobar resection	77	73	
Segmentectomy	6	15	
Wedge resection	13	8	

SUVmax, Maximum standardized uptake value; *N/A*, not applicable.

TABLE 4. Comparison between solid and mixed tumor characteristics in patients matched for solid component size and maximum standardized uptake value

	Solid tumor (n = 79)	Mixed tumor (n = 79)	*P*
Age (y)	64.4 ± 10.7	66.0 ± 8.9	.27
Sex			.62
Male	37 (46.8%)	41 (51.9%)	
Female	42 (53.2%)	38 (48.1%)	
Whole tumor size (cm)	1.8 ± 0.5	2.2 ± 0.5	<.001
Solid component size (cm)	1.8 ± 0.5	1.8 ± 0.5	N/A
SUVmax	3.7 ± 2.4	3.7 ± 2.6	N/A
Lymphatic invasion			.31
Negative	53 (67.1%)	60 (75.9%)	
Positive	26 (32.9%)	19 (24.1%)	
Vascular invasion			1.0
Negative	56 (70.9%)	56 (70.9%)	
Positive	23 (29.1%)	23 (29.1%)	
Pleural invasion			.71
Negative	62 (78.5%)	65 (82.3%)	
Positive	17 (21.5%)	14 (17.7%)	
Lymph node metastasis			.80
Negative	67 (84.8%)	69 (87.3%)	
Positive	12 (15.2%)	10 (12.7%)	
Procedure			.15
Lobar resection	61 (77.2%)	66 (83.5%)	
Segmentectomy	5 (6.3%)	8 (10.1%)	
Wedge resection	13 (16.5%)	5 (6.3%)	

SUVmax, Maximum standardized uptake value; *N/A*, not applicable.

In a next step, we evaluated whether mixed tumors exhibited malignant behavior and prognosis similar to those of solid tumors after matching for solid component size and SUVmax. In this matched model, solid tumors and mixed tumors had similar clinical characteristics and DFS. As shown in Figure 2, tumors with equivalent solid component size and SUVmax had the same malignant behavior (eg, lymphatic invasion), regardless of type. The DFS of patients with solid and mixed tumors was also comparable after matching for solid component size and SUVmax. These findings indicate that solid tumors and mixed tumors show similar biological behavior and prognosis when both have the same solid component size on HRCT and the same SUVmax value on PET/CT. In other words, solid component size on HRCT and SUVmax on PET/CT are important factors for evaluating malignant behavior of clinical stage IA lung adenocarcinomas before surgery, and this is regardless of the GGO proportion. Solid and mixed lung adenocarcinoma tumors with low SUVmax reflect pathologic noninvasiveness and may be good candidates for sublobar resection. We have previously reported, in the same population who were evaluated in the current study, that tumors with SUVmax less than 1.5 were not associated with lymph node metastasis or recurrence,[12,18] and we recommend that individuals with clinical stage IA lung adenocarcinomas with

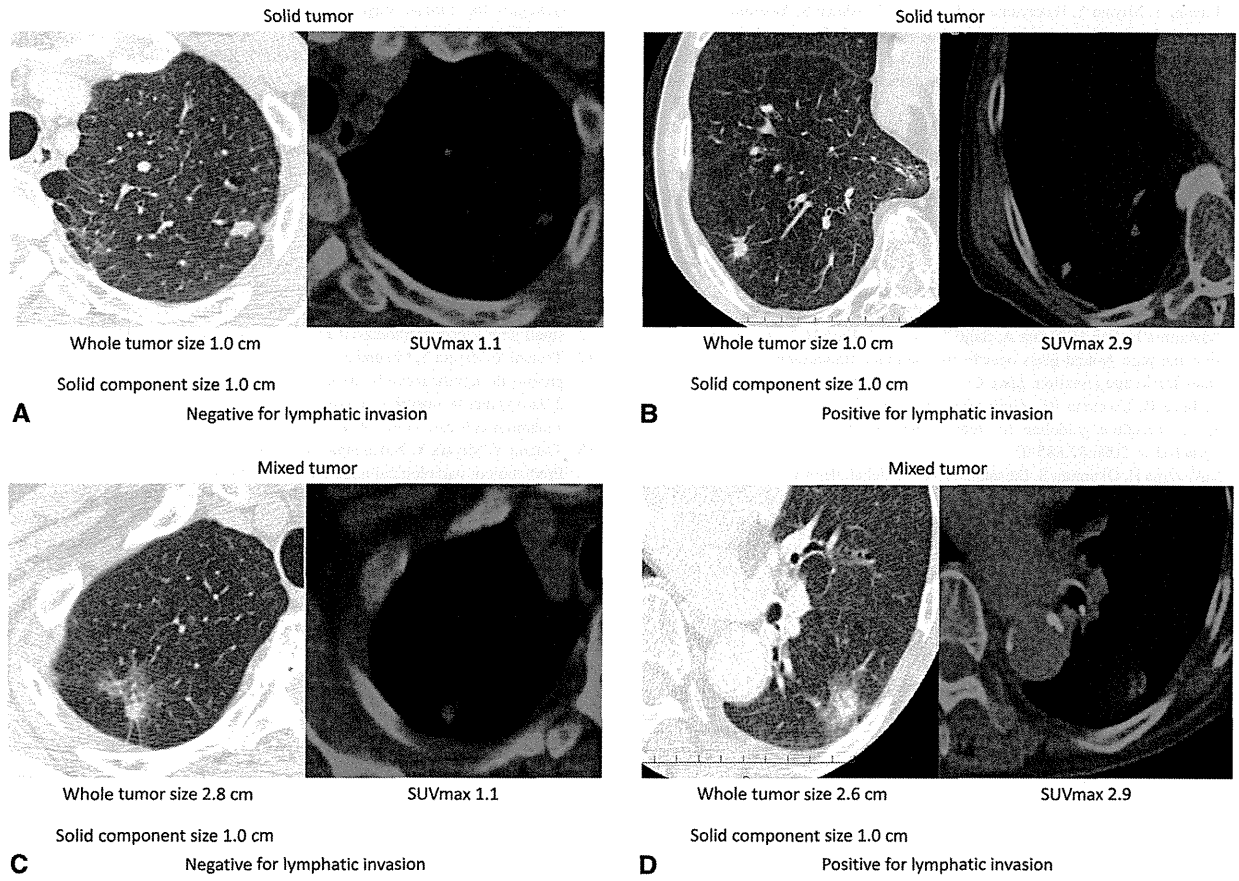

FIGURE 2. Examples of solid and mixed tumors on HRCT. A, Whole tumor size = solid component size: 1.0 cm, SUVmax: 1.1. This solid tumor was negative for lymphatic invasion. B, Whole tumor size = solid component size: 1.0 cm, SUVmax: 2.9. This solid tumor was positive for lymphatic invasion. C, Whole tumor size: 2.8 cm, solid component size: 1.0 cm, SUVmax: 1.1. This mixed tumor was negative for lymphatic invasion. D, Whole tumor size: 2.6 cm, solid component size: 1.0 cm, SUVmax: 2.9. This mixed tumor was positive for lymphatic invasion. *SUVmax,* Maximum standardized uptake value.

SUVmax less than 1.5 should undergo sublobar resection with adequate surgical margins.[18]

One of the strengths of this study is the use of PET/CT in all patients. PET/CT, which is the diagnostic tool of choice for patients with non–small cell lung cancer, improves the sensitivity of preoperative staging and reduces the frequency of futile thoracotomies.[19] In addition, SUVmax on PET/CT is a known prognostic factor for non–small cell lung cancer, especially for adenocarcinoma.[6,11,12,16,17] For patients with clinical stage IA lung adenocarcinoma who do not undergo PET/CT, tumor type (solid or mixed) is an important factor for predicting malignant behavior and prognosis. Because the follow-up period was short in this study, long-term follow-up is needed to confirm the DFS results.

CONCLUSIONS

In cases of clinical stage IA lung adenocarcinoma, solid tumors are more malignant than mixed tumors even after matching for solid component size in both tumor types. However, solid tumors have the same malignant potential and prognosis as mixed tumors when both tumor types are matched for solid component size on HRCT and SUVmax on PET/CT.

References

1. Okada M, Koike T, Higashiyama M, Yamato Y, Kodama K, Tsubota N. Radical sublobar resection for small-sized non-small cell lung cancer: a multicenter study. *J Thorac Cardiovasc Surg.* 2006;132:769-75.
2. Nakayama H, Yamada K, Saito H, Oshita F, Ito H, Kameda Y, et al. Sublobar resection for patients with peripheral small adenocarcinomas of the lung: surgical outcome is associated with features on computed tomographic imaging. *Ann Thorac Surg.* 2007;84:1675-9.
3. National Lung Screening Trial Research Team, Aberle DR, Adams AM, Berg CD, Black WC, Clapp JD, Fagerstrom RM, et al. Reduced lung-cancer mortality with low-dose computed tomographic screening. *N Engl J Med.* 2011;365:395-409.
4. Nakata M, Saeki H, Takata I, Segawa Y, Mogami H, Mandai K, et al. Focal ground-glass opacity detected by low-dose helical CT. *Chest.* 2002;121:1464-7.
5. Jang HJ, Lee KS, Kwon OJ, Rhee CH, Shim YM, Han J. Bronchioloalveolar carcinoma: focal area of ground-glass attenuation at thin-section CT as an early sign. *Radiology.* 1996;199:485-8.

6. Tsutani Y, Miyata Y, Nakayama H, Okumura S, Adachi S, Yoshimura M, et al. Prognostic significance of using solid versus whole tumor size on high-resolution computed tomography for predicting the pathological malignant grade of tumors in clinical stage IA lung adenocarcinoma: a multicenter study. *J Thorac Cardiovasc Surg*. 2012;143:607-12.
7. Goldstraw P, Crowley J, Chansky K, Giroux DJ, Groome PA, Rami-Porta R, et al. International Association for the Study of Lung Cancer International Staging Committee; Participating Institutions. The IASLC Lung Cancer Staging Project: proposals for the revision of the TNM stage groupings in the forthcoming (seventh) edition of the TNM Classification of Malignant Tumours. *J Thorac Oncol*. 2007;2:706-14.
8. Suzuki K, Asamura H, Kusumoto M, Kondo H, Tsuchiya R. "Early" peripheral lung cancer: prognostic significance of ground glass opacity on thin-section computed tomographic scan. *Ann Thorac Surg*. 2002;74:1635-9.
9. Nakamura H, Saji H, Ogata A, Saijo T, Okada S, Kato H. Lung cancer patients showing pure ground-glass opacity on computed tomography are good candidates for wedge resection. *Lung Cancer*. 2004;44:61-8.
10. Delbeke D, Coleman RE, Guiberteau MJ, Brown ML, Royal HD, Siegel BA, et al. Procedure guideline for tumor imaging with 18F-FDG PET/CT 1.0. *J Nucl Med*. 2006;47:885-95.
11. Nakayama H, Okumura S, Daisaki H, Kato Y, Uehara H, Adachi S, et al. Value of integrated positron emission tomography revised using a phantom study to evaluate malignancy grade of lung adenocarcinoma. *Cancer*. 2010;116:3170-7.
12. Okada M, Nakayama H, Okumura S, Daisaki H, Adachi S, Yoshimura M, et al. Multicenter analysis of high-resolution computed tomography and positron emission tomography/computed tomography findings to choose therapeutic strategies for clinical stage IA lung adenocarcinoma. *J Thorac Cardiovasc Surg*. 2011;141:1384-91.
13. Inoue M, Minami M, Sawabata N, Utsumi T, Kadota Y, Shigemura N, et al. Clinical outcome of resected solid-type small-sized c-stage IA non-small cell lung cancer. *Eur J Cardiothorac Surg*. 2010;37:1445-9.
14. Suzuki K, Kusumoto M, Watanabe S, Tsuchiya R, Asamura H. Radiologic classification of small adenocarcinoma of the lung: radiologic-pathologic correlation and its prognostic impact. *Ann Thorac Surg*. 2006;81:413-9.
15. Cerfolio RJ, Bryant AS, Ohja B, Bartolucci AA. The maximum standardized uptake values on positron emission tomography of a non-small cell lung cancer predict stage, recurrence, and survival. *J Thorac Cardiovasc Surg*. 2005;130:151-9.
16. Okada M, Tauchi S, Iwanaga K, Mimura T, Kitamura Y, Watanabe H, et al. Associations among bronchioloalveolar carcinoma components, positron emission tomographic and computed tomographic findings, and malignant behavior in small lung adenocarcinomas. *J Thorac Cardiovasc Surg*. 2007;133:1448-54.
17. Tsutani Y, Miyata Y, Misumi K, Ikeda T, Mimura T, Hihara J, et al. Difference in prognostic significance of maximum standardized uptake value on [18F]-fluoro-2-deoxyglucose positron emission tomography between adenocarcinoma and squamous cell carcinoma of the lung. *Jpn J Clin Oncol*. 2011;41:890-6.
18. Tsutani Y, Miyata Y, Nakayama H, Okumura S, Adachi S, Yoshimura M, et al. Prediction of pathological node-negative clinical stage IA lung adenocarcinoma for optimal candidates undergoing sublobar resection. *J Thorac Cardiovasc Surg*. 2012;144:1365-71.
19. Fischer B, Lassen U, Mortensen J, Larsen S, Loft A, Bertelsen A, et al. Preoperative staging of lung cancer with combined PET-CT. *N Engl J Med*. 2009;361:32-9.

GTS

Experimental and Molecular Pathology 94 (2013) 330–335

Contents lists available at SciVerse ScienceDirect

Experimental and Molecular Pathology

journal homepage: www.elsevier.com/locate/yexmp

The role of Necl-5 in the invasive activity of lung adenocarcinoma

Shinya Tane [a], Yoshimasa Maniwa [a,*], Daisuke Hokka [a], Shunsuke Tauchi [a], Wataru Nishio [b], Yutaka Okita [c], Masahiro Yoshimura [a,b]

[a] Division of Thoracic Surgery, Kobe University Graduate School of Medicine, Japan
[b] Division of Thoracic Surgery, Hyogo Cancer Center 13-70, Kitaoji-cho, Akashi, Hyogo prefecture, 673-8558, Japan
[c] Division of Cardiovascular Surgery, Kobe University Graduate School of Medicine 7-5-2, Kusunoki-cho, Chuo-ku, Kobe, 650-0017, Japan

ARTICLE INFO

Article history:
Received 20 August 2012
and in revised form 16 November 2012
Available online 28 December 2012

Keywords:
Necl-5
Invasion
Lung adenocarcinoma
Cancer–stromal interaction

ABSTRACT

Nectin-like molucule-5 (Necl-5) is an immunoglobulin-like molecule that was originally identified as a poliovirus receptor and is often upregulated in cancer cells. It has been said that Necl-5 plays a role in not only cell–cell adhesion, but also cell migration, proliferation, and metastasis. In this study, we used a bronchioloalveolar carcinoma (BAC) cell line and fibroblasts to assess the expression of Necl-5 in the development of cancer–stroma communication by using an easy-to-prepare double-layered collagen gel hemisphere (DL-CGH) system that enables visualization of cell migration during invasion. The expression of Necl-5 was higher in BAC cells than in fibroblasts. This tendency didn't change even when the BAC cells were mixed with fibroblasts. To assess the role of Necl-5 in the invasive activity of the BAC cells, we knocked down its expression using RNA interference (RNAi). The invasion assay with DL-CGH revealed that inhibition of Necl-5 expression in the BAC cells was associated with suppressed invasiveness. In addition, Necl-5 knockdown inhibited the movement and proliferation of the BAC cells. Necl-5 expression in lung cancer cells is crucial for their invasiveness in the cancer–stromal interaction, suggesting that Necl-5 could be a favorable molecular target for the suppression of invasiveness in lung adenocarcinoma.

Introduction

Nectins, which are Ca^{2+}-independent cell–cell adhesion molecules, are instrumental in the formation of cadherin-based adherens junctions in fibroblasts and epithelial cells (Takai et al., 2003, 2008). Recently, the role of nectin-like molecules (Necl), which have been characterized on the basis of their structural similarity to nectin and their function in cell–cell adhesion, has been clarified (Ikeda et al., 2003; Miyoshi and Takai, 2007; Takai et al., 2008). Necl-5, one of the Necl family members, is preferentially localized at the leading edge of moving cells where it promotes cell movement and proliferation (Ikeda et al., 2003; Kakunaga et al., 2004; Miyoshi and Takai, 2007; Sato et al., 2004; Takai et al., 2008). The expression of Necl-5 is downregulated when cultured cells become confluent, resulting in the suppression of cell movement and proliferation (Fujito et al., 2005). Thus, down-regulation of Necl-5 is, at least in part, one mechanism that underlies contact inhibition of cell movement and proliferation.

Necl-5 is overexpressed in various human carcinomas (Chadeneau et al., 1994; Faris et al., 1990; Koike et al., 1990; Lim et al., 1996), and experiments using transformed and cancer cell lines that express Necl-5 have shown that the downregulation of Necl-5 in these cells decreases migration, proliferation, and metastasis (Ikeda et al., 2003; Kakunaga et al., 2004; Sloan et al., 2004). We previously showed that overexpression of Necl-5 in cancer cells had clinical significance for poor prognosis in lung adenocarcinoma patients (Nakai et al., 2010). Furthermore, microscopic observation revealed that the Necl-5 was strongly stained in the invasive sites of the tumors, where stromal cells and cancer cells were mixed in a disorderly pattern.

Clinical studies demonstrated that a poor prognosis for patients with bronchioloalveolar carcinoma (BAC) depended on the presence of proliferating stromal fibroblasts (Noguchi et al., 1995). Our previous in vitro experiments showed that the invasive migration of A549 BAC cells depended on the presence of fibroblasts (Takata et al., 2007). These findings suggested that cancer–stromal interactions play an important role in the infiltration of BAC cells. Because Necl-5 was strongly expressed in the invasive front of BAC, we hypothesized that the control of Necl-5 in lung adenocarcinoma would inhibit the cancer–stromal interaction, resulting in inhibition of cancer cell migration and proliferation. In the present study, we assessed the role of Necl-5 in cancer–stromal interactions by using the simple 3-D invasion assay that we established previously (Doi et al., 2011; Takata et al., 2007).

Material and methods

Cell lines

The A549 BAC cell line was obtained from the Cell Resource Center for Biomedical Research, Institute of Development, Aging and Cancer, Tohoku University; the WI-38 (lung fibroblast) cell line was obtained

* Corresponding author. Fax: +81 78 382 5959.
E-mail address: maniwa@med.kobe-u.ac.jp (Y. Maniwa).

0014-4800/$ – see front matter © 2013 Elsevier Inc. All rights reserved.
http://dx.doi.org/10.1016/j.yexmp.2012.12.003

from the Health Science Research Resources Bank (Osaka, Japan); the green fluorescent protein (GFP)-labeled A549 BAC cell line was obtained from AntiCancer Corp. (Osaka, Japan). Cells were maintained in RPMI-1640 medium supplemented with penicillin (100 U/ml), streptomycin (100 U/ml), and 10% bovine calf serum (at 37 °C, 5% CO_2).

Western blotting

Cultured cells were washed with phosphate buffered saline (PBS) and then lysed with 100 μl Laemmli sample buffer, after which 10 μl of the samples were separated using SDS-PAGE. The separated proteins were then transferred to nitrocellulose membranes (GE Healthcare Corp.), which were washed with PBS-T and then blocked for 30 min with a PBS-T solution containing 5% skim milk. Blocked membranes were then rinsed twice with PBS-T and incubated (1 h, room temperature) with Necl-5 primary antibody (#ab103630; Abcam, Cambridge, UK) and focal adhesion kinase (FAK) primary antibody (#ab4803; Abcam, Cambridge, UK), which were diluted 1:500 with 5% BSA/PBS-T. FAK is a tyrosine kinase that resides at the sites of focal adhesion, which has been shown to be an important mediator of cell adhesion and migration (Golubovskaya, 2010). After the membranes were washed with PBS-T, membranes were incubated (30 min, room temperature) with the secondary peroxidase-labeled donkey anti-rabbit Ig whole antibody (GE Healthcare Corp.), which was diluted 1:5000 with PBS-T. Membranes were washed with PBS-T and then treated with a chemiluminescent detection kit (GE Healthcare Corp.) before they were visualized using a luminoimage analyzer (LAS-3000; Fujifilm Inc., Tokyo, Japan).

As a control assay, immunoblotting was performed on the same membranes with a primary antibody directed against β-actin (#4967, Cell Signaling Technology), followed by a peroxidase-labeled donkey anti-rabbit Ig whole secondary antibody (GE Healthcare Corp.).

Preparation of a double-layered collagen gel hemisphere (DL-CGH)

Acid-soluble collagen 1 (Nitta Gelatin Inc., Osaka, Japan), 10-fold concentrated Ham's F-12 medium, and reconstruction buffer (2.2 g $NaHCO_3$ + 4.77 g HEPES in 100 ml of 0.05-N NaOH) were mixed in a volume ratio of 8:1:1 and then seeded with cells cultured at a density of 3.0×10^6 cells/ml. Five microliters of the mixture containing 3.0×10^4 cells was then dropped onto a plastic dish. Once the mixture had gelled, a second 30-μl drop of collagen was placed directly on the top of the first gel drop, encapsulating it completely. The gel hemisphere was then submerged in medium and cultured.

RNA interference (RNAi) in the A549 BAC cell lines

RNAi was performed with commercially available siRNA for Necl-5 (target sequence, CAG GCT ATA ATT GAA GCA CGA; Qiagen GmbH) and a non-silencing control siRNA (AllStars Negative Control siRNA; Qiagen GmbH) according to the manufacturer's instructions. Briefly, 20 μl of transfection reagent (Hiperfect; Qiagen GmbH) was suspended in 200 μl of serum-free culture medium containing 2.5 μM siRNA. After a 10-min incubation at room temperature, the mixture was added to A549s (60-mm round dish with 4 ml culture medium containing 10% fetal bovine serum and antibiotics mentioned above) grown to 80% confluence; the final concentration of the siRNA was 100 nM. After 24 h (at 37 °C, 5% CO_2), these cells were suspended in PBS, and the cell density was calculated to prepare for the encapsulation of the cells in DL-CGH.

Evaluation of A549 and WI-38 cell invasion

To observe the activity of Necl-5 in the interaction between GFP-labeled A549s and WI-38s, 1.5×10^4 cells of each type were mixed in the first gel layer and incubated for 4 days. The invasion activity of the cells was then evaluated by counting the GFP-labeled A549s in the outer collagen layer by using a BZ9000 fluorescence microscope (Keyence Corp., Tokyo, Japan). In separate experiments, GFP-labeled A549s were first transfected with either inhibitory RNA for Necl-5 or non-silencing control siRNA before they were embedded in the first gel layer. The invasion activity of the transfected cells was then compared.

Time-lapse motion picture of the cell movement

A BZ9000 fluorescence microscope with a CO_2 chamber was used to evaluate cell movement. DL-CGH prepared on a 35-mm round plastic dish with 2 ml medium was mounted on the microscope-table incubation chamber, and a 10× objective image was displayed on the monitor. Recording started at 48 h after DL-CGH culture initiation, and continued for 12 h. The movement of the GFP-labeled A549s was then calculated. In addition, 20× fluorescent images of the GFP-labeled A549 were captured every hour from 48 h after culture initiation to 168 h, and stored as 1360×1024-pixel TIFF files. A movie (saved as an MPEG-2 file) was then created, which displayed 120 consecutive images, with 0.2 s per image, by using the EDIUS ver.5.0 software (Grass Valley K.K., Kobe, Japan).

Statistical analysis

Statistical significance was determined using unpaired Student's *t*-test. All tests were performed with JMP ver. 8.0 statistical software (SAS Japan Institute Inc., Tokyo, Japan).

Results

Necl-5 expression in cancer cells and normal fibroblasts

Western blotting was performed to determine whether Necl-5 and FAK were expressed in the cell lines of bronchioloalveolar carcinoma (A549), fibroblast (WI-38), and a mixture of each cell type. We detected strong expression of Necl-5 in the A549 cell line. However, the expression of Necl-5 was very weak in WI-38s. In the mixture of A549 and WI-38, Necl-5 was moderately expressed. FAK expression showed the same tendency of Necl-5 (Fig. 1). These findings suggest that both Necl-5 and FAK are strongly expressed in A549s in both the absence and presence of WI-38s.

Effect of RNAi-mediated knockdown of Necl-5 on the invasive activity of cancer cells

We previously showed that A549 cells, which were unable to infiltrate the outer layer alone, opportunistically invade along the paths of infiltrating WI-38s in the DL-CGH test. We therefore decided to use this assay to assess if the invasive activity of A549 cell lines is controlled by Necl-5 by inhibiting expression of Necl-5 in A549s. Initial knockdown studies showed that cells transfected with Necl-5 siRNA have a 50% reduction in the expression of both Necl-5 and FAK protein relative to cells transfected with control siRNA (Fig. 2). In the DL-HCG test, GFP-labeled A549 transfected with Necl-5 RNAi and GFP-labeled A549 transfected with control non-silencing siRNA were mixed with WI-38 in the inner layer. After 4 days of incubation, invasive activity (represented by the number of GFP-labeled A549 in the outer collagen layer) was measured. The number of A549 cells in the group transfected with Necl-5 RNAi showed a significant decrease relative to the number in the non-treated group or the group transfected with control non-silencing siRNA (Figs. 3 and 4). Thus, inhibition of Necl-5 in A549 resulted in suppressed invasive activity.

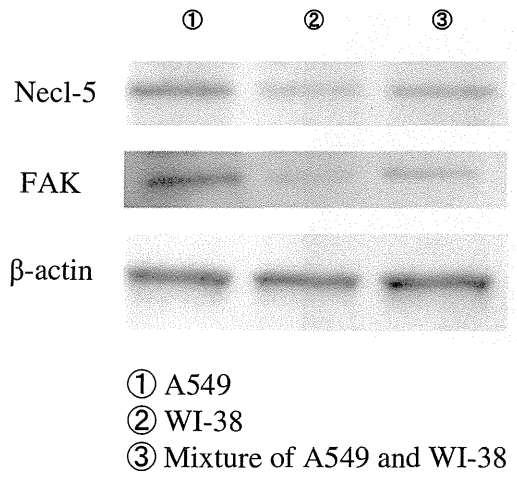

Fig. 1. *Western blotting for Necl-5, FAK and β-actin.* Expression of Necl-5 was stronger in A549 cells than in WI-38 cells. In the mixture of A549s and WI-38s, Necl-5 was moderately expressed. FAK expression showed the same tendency of Necl-5.

Effect of RNAi-mediated knockdown of Necl-5 on cell proliferation

Since it is difficult to evaluate proliferation using the DL-HCG model, we assessed the proliferative effects of Necl-5 on A549s on normal tissue culture plates (60-mm-round dish with 4-ml culture medium containing 10% fetal bovine serum and antibiotics as mentioned above) containing 40×10^4 A549s cells transfected with either Necl-5 RNAi or control non-silencing siRNA. The number of cells in each transfected cell line was counted every 24 h from culture initiation up until 72 h. The cells transfected with Necl-5 RNAi grew more slowly when compared to the other cell lines (Fig. 5), which reveals that the knockdown of Necl-5 inhibits proliferation of A549 cells.

Effect of RNAi-mediated knockdown of Necl-5 on cell movement

The cell movement of GFP-labeled Necl-5 transfected A549s was also evaluated, because invasiveness in the DL-CGH models might be affected by rates of proliferation. As noted above, we created 3 types of DL-CGH models (GFP-labeled A549, A549s transfected with Necl-5 RNAi, and A549s transfected with control non-silencing siRNA, each mixed with fibroblasts in the inner layer). In this study, we then observed GFP-labeled A549 movement over 12 h by using the time-lapse method and compared the migration distance in each models

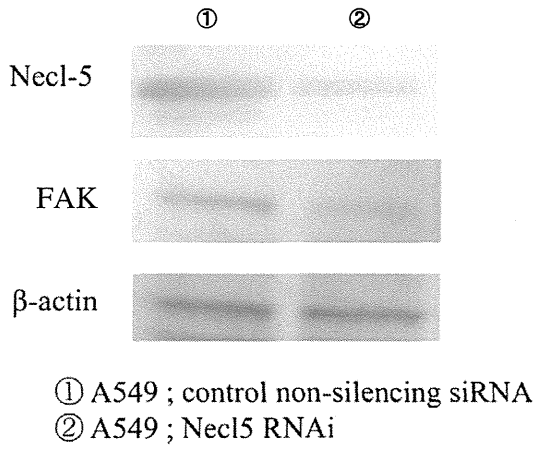

Fig. 2. *Western blotting after transfection with Necl-5 RNAi.* Immunoblotting showed a 50% reduction in the expression of both Necl-5 and FAK proteins relative to cells transfected with control non-silencing siRNA.

(Fig. 6a). Compared to other models, these models revealed that A549s transfected with Necl-5 RNAi moved more slowly along the surfaces of the fibroblasts (Fig. 6b).

Discussion

Necl-5, which was previously named Tage4, plays a role not only in cell–cell adhesion, but also in cell migration, proliferation, and metastasis (Ikeda et al., 2003; Kakunaga et al., 2004; Miyoshi and Takai, 2007; Morimoto et al., 2008; Sato et al., 2004; Takai et al., 2008). Necl-5 colocalizes with integrin αvβ3 at the leading edges of moving cells (Ikeda et al., 2004), and through activation of Cdc42 and Rac, induces the formation of filopodia and lamellipodia, which eventually enhance growth factor-induced cell movement (Takai et al., 2001). In addition, Necl-5 also enhances the proliferation induced by growth factor receptors, such as PDGF and FGF (Kakunaga et al., 2004), and through activation of the Ras–Raf–MEK–ERK signaling, causes upregulation or downregulation of the cell cycle regulators, including cyclins D2, E, and p27kip1. These effects contribute to shortening of the G1 phase of the cell cycle and enhancement of growth factor-induced cell proliferation. Necl-5 does not show any homophilic cell–cell adhesion activity, but does heterophilically trans-interact with nectin-3 (Ikeda et al., 2003). When cells come into contact with other cells, Necl-5 is downregulated from the cell surface by its trans-interaction with nectin-3, thereby leading to inhibition of cell migration and proliferation (Fujito et al., 2005; Sato et al., 2004). Transformation of cells, which induces high levels of Necl-5 expression, causes disruption of cell–cell adhesion, increase of cell motility, and loss of contact inhibition of cell movement and proliferation, eventually leading to cancer invasion.

Necl-5 is highly expressed in various cancer cell lines and human cancer tissues (Chadeneau et al., 1994; Faris et al., 1990; Ikeda et al., 2003; Koike et al., 1990; Lim et al., 1996; Nakai et al., 2010; Sloan et al., 2004). We previously reported that the abnormal overexpression of Necl-5 in cancer cells has negative prognostic factors for primary lung adenocarcinomas (Nakai et al., 2010). According to this report, the microscopic observation of immunostaining revealed that Necl-5 was strongly expressed especially in the peripheral area of the BAC, where cancer cells infiltrated aggressively into the stroma, but not at the tumor center in many of the BACs. Tokunou et al. have reported the importance of cancer–stromal communication for the development of the invasive component of BAC (Tokunou et al, 2001). We assumed that such overexpression of Necl-5 might play a role in the aberrant behavior at the invasive front of BAC, and set out to assess the activity of Necl-5 in the development of cancer–stromal communication by in vitro analysis. In this study, we revealed that inhibition of Necl-5 in cancer cells reduced their invasiveness and proliferation. However, Necl-5 physiologically suppresses cell movement and proliferation in normal cell–cell contact (Fujito et al., 2005). It is still not clear why this normal function of Necl-5 was lost in the cancer–stromal interaction.

Cell migration is a complex so-called "adhesion turnover" process that involves the continuous formation and disassembly of adhesions. Adhesion formation takes place at the leading edge of cell protrusions, whereas disassembly occurs both at the cell near and at the base of protrusion. FAK is known to be crucial for adhesion turnover at the cell front, a process central to migration. Normal tissues have low expression of FAK, while cancer cells significantly overexpress this protein (Golubovskaya, 2010; Webb et al., 2004). In this study, both Necl-5 and FAK are strongly expressed in A549s in both the absence and presence of WI-38s. Moreover, A549s transfected with Necl-5 siRNA have a 50% reduction in the expression of both Necl-5 and FAK proteins. These results supported that the overexpression of Necl-5 in cancer cells might be related to FAK in cancer cell migration.

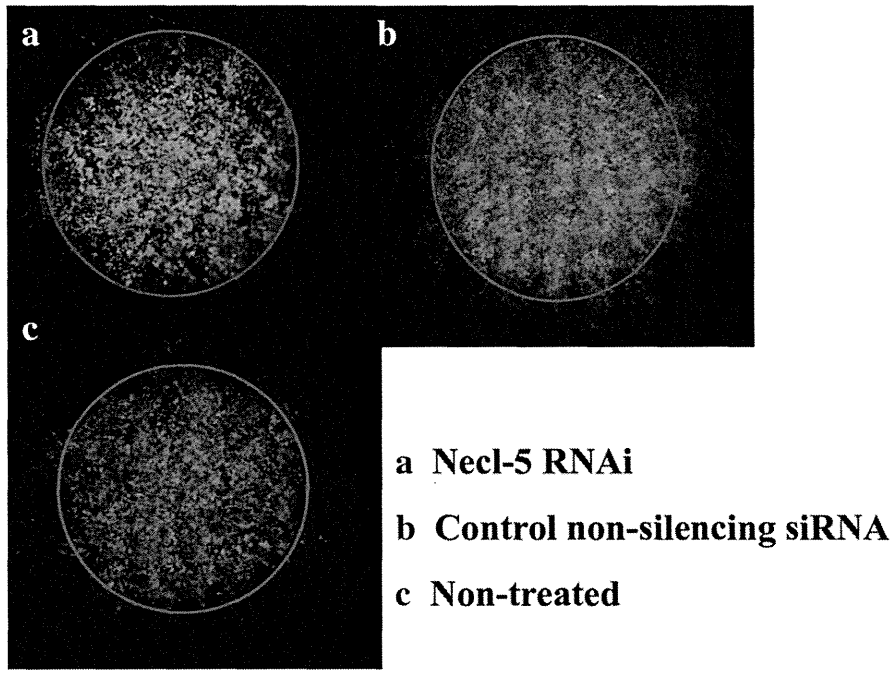

Fig. 3. *Results from the DL-CGH assay using GFP-labeled A549s and WI-38 in the inner layer.* Each cell line ((a) A549s transfected with Necl-5 RNAi, (b) A549s transfected with control non-silencing siRNA, and (c) non-treated A549s) was mixed with WI-38s in the inner layer (blue line). A549s transfected with Necl-5 RNAi showed less invasiveness into the outer layer relative to the other cell lines.

The differences among the different tissue types of human lung adenocarcinoma, such as BAC, papillary, acinar, and solid carcinomas, remained controversial in clinical practice (Kerr, 2009). Human lung adenocarcinomas are often composed of mixed components of these tissue types. Noguchi et al. (1995) reported that patients with BAC containing actively proliferating fibroblasts show a worse prognosis than do patients with small-sized BAC, in which cancer cells spread on the internal surface of alveoli but do not infiltrate interstitially. This result was consistent with the fact that the abnormal overexpression of Necl-5 in the invasive front of cancer cells in primary lung adenocarcinomas negatively affects the prognosis of patients.

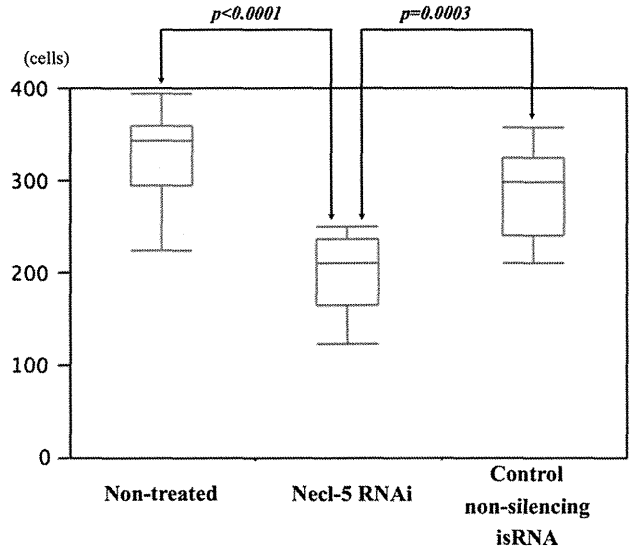

Fig. 4. *Comparison of A549 invasive activity by using the DL-CGH assay (represented by the number of GFP-labeled A549s in the outer collagen layer).* A549 cells transfected with Necl-5 RNAi showed a significant decrease in invasive activity relative to the non-treated group ($p<0.0001$) or control non-silencing siRNA transfected group ($p=0.0003$) ($n=10$ samples for each group).

Many studies have shown that disruption of cell–cell adhesion of tumor epithelial cells, resulting in epithelial–mesenchymal transition (EMT), causes tumor progression and is highly related to poor prognosis for cancer patients (Bellovin et al., 2005; Shioiri et al., 2006; Soltermann et al., 2008; Thiery, 2002). Liotta et al. demonstrated that cancer invasion occurs within a tumor–host microecology, where stroma and tumor cells exchange enzymes and cytokines that modify the local extracellular matrix, stimulate migration, and promote proliferation and survival (Liotta and Kohn, 2001). Thus, the presence of fibroblasts is essential for cancer invasion. In fact, we showed that A549s (BAC) in the inner layer of the DL-CGH model could not infiltrate into the outer layer by themselves, whereas A549 mixed with WI-38 (fibroblast) widely spread into the outer layer (data not shown). Moreover, the A549 BAC cells, like amoebas, move and spread along the fibroblasts (Takata et al., 2007). This fact

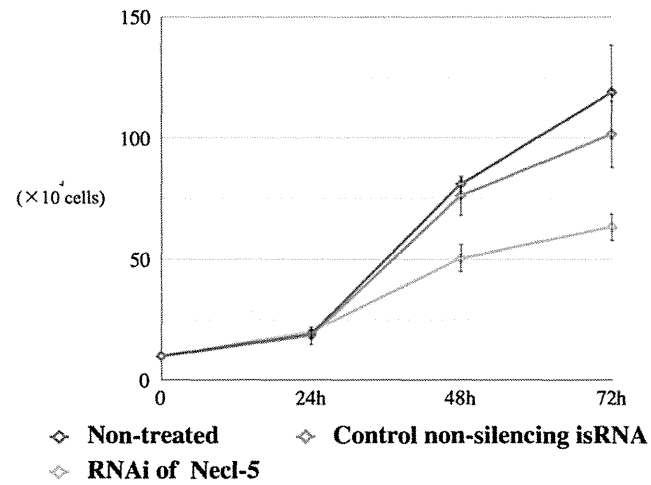

Fig. 5. *Comparison of Necl-5-transfected A549 proliferative activity.* A549 cells transfected with Necl-5 RNAi grew slower compared to normal cells and control-treated cells ($n=5$ samples for each group).